

Master's Thesis

Adaptive Beamforming for Next Generation Cellular System

Sebastian Andersson
William Tidelund



DEPARTMENT OF ELECTRICAL AND INFORMATION TECHNOLOGY
FACULTY OF ENGINEERING | LTH | LUND UNIVERSITY
SE-221 00 LUND, SWEDEN

Adaptive Beamforming for Next Generation Cellular System

Sebastian Andersson elt11sa1@student.lu.se
William Tidelund elt11wti@student.lu.se

September 16, 2016

Supervisors

Fredrik Tufvesson fredrik.tufvesson@eit.lth.se
Harish Venkatraman Bhat harish.venkatraman.bhat@ericsson.com

Ericsson
Mobilvägen 1, 224 71 Lund

ABSTRACT

In this work a Matlab model of a simplified LTE system has been implemented. The PUSCH and PDSCH signal chains has been used for reception and transmission of data and DM-RS symbols are used as pilots. Moreover, the model supports communication and interference between multiple users and base station antennas. The wireless channels are modeled as multi-path Rayleigh fading and are continuous in time such that multiple frames can be transmitted on a correlated channel. Three standardized multi-path delay profiles have been used for modeling users in pedestrian, vehicular and urban environments. Three beamforming algorithms have been implemented, maximum ratio transmission, zero-forcing and regularized zero-forcing. This model is an extension to the current standard of LTE in the sense that the parameters of the model are scalable beyond what is currently in the standard. The different algorithms are compared in many different scenarios, including different modulation levels, delay profiles, number of user sharing the same resources, number of base station antennas, multi-layer transmissions and complexity. Maximum ratio transmission is shown to be computationally less complex, while the zero-forcing algorithms is better at removing inter-user interference, especially as the number of users sharing the same resources grows for a constant number of base station antennas. Regularized zero-forcing is shown to outperform the other algorithms when looking at the entire SNR range.

ACKNOWLEDGEMENTS

We would like to thank Marcus Wiedner, Harish Venkatraman Bhat, Johan Åman and Christer Östberg who gave us the opportunity to do this Master's thesis at Ericsson and who also provided us with valuable feedback during the work. Also a big thanks to Fredrik Tufvesson and his inputs to the thesis work as one of the leading researchers in this area. We are glad that we had the opportunity to do our thesis in this area even though our knowledge in telecommunications was limited before starting, because we've learned so much of this ever-expanding subject.

Finally a big thanks to family and friends who have supported us during the entire time of studies.

William Tidelund & Sebastian Andersson

CONTENTS

1 Introduction	1
1.1 Purpose & Aims	1
1.2 Methodology	1
1.3 Limitations	2
1.4 Literature Study	2
2 Background	3
2.1 Uplink and Downlink	3
2.2 LTE Resources	4
2.3 Transmission of User Data	5
2.4 Reception of User Data	8
2.5 Reference Signals	9
3 Wireless Channel	11
3.1 Channel Model	11
3.1.1 Fading Model	11
3.1.2 Time Correlation	12
3.1.3 Filter Structure & Spatial Correlation	13
3.1.4 Large Scale Fading	15
3.1.5 Path Loss	15
3.2 Uplink and Downlink Reciprocity	15
3.3 Noise	16
3.4 Coherence Time	16
4 Downlink Beamforming	17
4.1 Maximum Ratio Transmission	19
4.2 Zero-Forcing	19
4.3 Regularized Zero-Forcing	20
4.4 Massive MIMO	20
4.5 Power Allocation	20
5 Modeling Using LTE System Toolbox in Matlab	23
5.1 Interface	23
5.1.1 Channel Setup	24
5.1.2 Link Setup and Transmission	24
5.2 Uplink	25
5.3 Channel	25
5.4 Downlink	28
6 Results	29
6.1 Throughput and Validation	29
6.2 Performance in Massive MIMO	33
6.3 Multi-Layer Transmission	34
6.4 Transmission of Consecutive Frames	35
6.5 Algorithm Complexity	37

6.6	Effects of Channel Discrepancies Between Users	37
6.7	Algorithm Performance and SNR	39
6.8	Antenna Correlation	40
6.9	Mobility	40
6.10	Effects of Large Scale Fading	42
7	Discussion	43
7.1	Conclusion	44
7.2	Future work	44

LIST OF FIGURES

1	Illustration of a LTE radio frame and its subcomponents, [8].	4
2	Six users in a 1.4 MHz bandwidth subframe.	5
3	Transmitter chain [13].	6
4	Constellation diagram QPSK.	6
5	Constellation diagram 16QAM.	6
6	Constellation diagram 64QAM.	7
7	Constellation diagram 256QAM.	7
8	Receiver chain [13].	8
9	User allocation for six users in a 1.4 MHz bandwidth UL subframe.	10
10	Signal envelope for 0.1 seconds with a maximum Doppler frequency of 70 Hz.	13
11	Signal envelope for 0.1 seconds with a maximum Doppler frequency of 300 Hz.	13
12	MIMO channel between one user and base station.	13
13	Time-varying FIR filter structure used for the channel.	14
14	GUI.	23
15	The program flow of the channel model, "LTESStep" in context.	27
16	Spectral efficiency as a function of UEs with QPSK and 32 ENB antennas on an EPA channel.	30
17	Spectral efficiency as a function of UEs with 256QAM and 32 ENB antennas on an EPA channel.	30
18	Spectral efficiency as a function of UEs with QPSK and 32 ENB antennas on an EVA channel.	30
19	Spectral efficiency as a function of UEs with 256QAM and 32 ENB antennas on an EVA channel.	30
20	Spectral efficiency as a function of UEs with QPSK and 32 ENB antennas on an ETU channel.	31
21	Spectral efficiency as a function of UEs with 256QAM and 32 ENB antennas on an ETU channel.	31
22	BER as a function of UEs with QPSK and 32 ENB antennas on an EPA channel.	32
23	BER as a function of UEs with 256QAM and 32 ENB antennas on an EPA channel.	32
24	BER as a function of UEs with QPSK and 32 ENB antennas on an EVA channel.	32
25	BER as a function of UEs with 256QAM and 32 ENB antennas on an EVA channel.	32
26	BER as a function of UEs with QPSK and 32 ENB antennas on an ETU channel.	33
27	BER as a function of UEs with 256QAM and 32 ENB antennas on an ETU channel.	33
28	Spectral efficiency for 4 UEs with QPSK on an EPA channel as the number of ENB antennas grows.	33

29	Spectral efficiency for 4 UEs with QPSK on an EVA channel as the number of ENB antennas grows.	33
30	Spectral efficiency for 4 UEs with QPSK on an ETU channel as the number of ENB antennas grows.	34
31	Spectral efficiency for 4 UEs using QPSK and 32 antennas on an EPA channel as the number of layers increases.	35
32	Spectral efficiency for 4 UEs using QPSK and 32 antennas on an EVA channel as the number of layers increases.	35
33	Spectral efficiency for 4 UEs using QPSK and 16 antennas on an EPA channel as the number of layers increases.	35
34	Spectral efficiency for 4 UEs using QPSK and 16 antennas on an EVA channel as the number of layers increases.	35
35	The DL BER with QPSK on an EVA channel as a function of consecutive DL frames.	36
36	The DL BER with QPSK on an ETU channel as a function of consecutive DL frames.	36
37	The DL BER using QPSK on an EVA channel as a function of subframes when the weights are updated every third subframe.	36
38	The DL BER using QPSK on an ETU channel as a function of subframes when the weights are updated every third subframe.	36
39	Computation time as the number of UEs and ENB antennas grows.	37
40	Received constellation of user 1 in a system with two users close to the base station.	38
41	Received constellation of user 2 in a system with two users close to the base station.	38
42	Received constellation of user 1 in a system with one user close to the base station and one further away.	38
43	Received constellation of user 2 in a system with one user close to the base station and one further away.	38
44	Received constellation of user 1 in a system with one user close to the base station and one very far away.	39
45	Received constellation of user 2 in a system with one user close to the base station and one very far away.	39
46	4 base station antennas.	40
47	32 base station antennas.	40
48	SE plotted against Doppler frequency.	41
49	Spread of the large scale fading around a mean path loss of -100 dB and a standard deviation of 4 dB.	42
50	Spread of the large scale fading around a mean path loss of -100 dB and a standard deviation of 10 dB.	42

LIST OF TABLES

1	Subcarriers and resource blocks as a function of the channel bandwidth, [5].	3
2	Codeword-to-layer mapping [9].	7
3	Parameters for the different delay profiles specified in LTE [18].	12
4	Correlation levels specified in LTE [18].	15
5	Throughput for the three specified correlations.	40

PREFACE

Systems and signals are things that amuse us; it is fun to build up a model of a system and then apply an algorithm to improve the system performance. Wireless MIMO and beamforming is the perfect example of such a system and we have had a great time working in this area. Even though we have worked with our thesis project for almost half a year it is hard to grasp that this actually works in reality and all the functionality that works together to give smartphones access to Internet almost anywhere at any time is astounding. In this Master's thesis project, William has done most of the work with the signal chains and beamforming algorithms while Sebastian focused more on channel modelling and building the GUI. The remaining parts have been done together and we have had discussions with each other throughout the entire work and both of us know the different areas of the work.

LIST OF ABBREVIATIONS

3GPP	3d Generation Partnership Project
AWGN	Additive White Gaussian Noise
BER	Bit Error Rate
CDM	Code Division Multiplexing
CRC	Cyclic Redundancy Check
CRZF	Complexity Reduced Zero-Forcing
DL	Downlink
DM-RS	Demodulation Reference Signal
ENB	Evolved Node B
EPA	Extended Pedestrian A model
ERP	Equal Receive Power
ETP	Equal Transmit Power
ETU	Extended Typical Urban model
EVA	Extended Vehicular A model
FDD	Frequency Division Duplex
FDM	Frequency Division Multiplexing
FFT	Fast Fourier Transform
FSPL	Free Space Path Loss
GUI	Graphical User Interface
IFFT	Inverse Fast Fourier Transform
i.i.d	Independent and Identically Distributed
LTE	Long Term Evolution
MIMO	Multiple-Input Multiple-Output
MMSE	Minimum Mean-Squared Error
MRT	Maximum Ratio Transmission
MU	Multi-User
OCC	Orthogonal Cover Code
OFDMA	Orthogonal Frequency Division Multiple Access
PDSCH	Physical Downlink Shared Channel
PUSCH	Physical Uplink Shared Channel
QAM	Quadrature Amplitude Modulation
QPSK	Quadrature Phase-Shift Keying
RB	Resource Block
RE	Resource Element
RZF	Regularized Zero-Forcing
SCFDMA	Single Carrier Frequency Division Multiple Access
SD	Standard Deviation
SE	Spectral Efficiency
SINR	Signal to Interference and Noise Ratio
SNR	Signal to Noise Ratio
TDD	Time Division Duplex
TM	Transmission Mode
UE	User Equipment
UL	Uplink
ZF	Zero-Forcing

1 INTRODUCTION

Our way to communicate with each other has rapidly changed over the past years. As more and more devices are connected to the Internet and are using applications that require more data, such as streaming, higher data rates are needed to support the everyday use. Thanks to long term evolution (LTE) and long term evolution advanced (LTE-A), we are no longer required to be connected to WiFi to achieve these data rates and you can move around in big areas without losing your connection. With support for high frequencies, many users and multiple sorts of multiple-input multiple-output (MIMO) techniques, the rates are constantly increasing. With the next generation of LTE beamforming will be used to increase the data rates. The general idea of beamforming is that each base station antenna transmits a phase shifted version of the same signal. If the beamforming weights that phase shifts the signals are found correctly, the received signal strength is increased. This is useful when the signal to noise ratio is low due to, for example, the user being far away or in a complex environment with multiple paths and interference. With a beamforming algorithm such as zero-forcing (ZF) the data rates can also be increased by cancelling inter-user interference. In the same way as you focus the beam in a certain direction you can also cancel it in other directions.

1.1 PURPOSE & AIMS

In this thesis work we investigate how beamforming can be done in an LTE system by building an LTE simulation model and run beamforming algorithms in this model. Different forms of beamforming are investigated, implemented and compared. The comparison of the algorithms is in terms of complexity, how they perform in different environments, for how long the beamforming weights are valid and how the performance changes with the ratio between the number of users and base station antennas. Multilayer transmission is also investigated and multilayer transmission is referred to as the amount of shared resources that can be transmitted to one user.

1.2 METHODOLOGY

To find an answer to the statements in Section 1.1, this thesis work begins with a literature study. Then an LTE based uplink (UL) and downlink (DL) model between multiple users and base station antennas is implemented. When the model is working, beamforming algorithms are investigated and integrated into the model. The model is built in Matlab and functions from the LTE System toolbox [1] are used to make the implementation easier. As this thesis focuses on beamforming in LTE systems, the model includes the necessary LTE functions to demonstrate and perform beamforming. The goal with the model is that it should include time division duplex (TDD) transmission and the following parameters; 20 MHz bandwidth (BW), at least 32 physical base station antennas, multiple users and multiple transmission layers.

1.3 LIMITATIONS

In this work the focus is on transmission to and from a single base station within a single cell. Furthermore, the users are assumed to have established a communication with the base station and therefore only data symbols and pilot symbols are transmitted on the link. Every user is also assumed to have the same amount of antennas to simplify the model. Moreover scheduling, error correction and retransmissions are not implemented to keep the model simple and to focus on the beamforming part. Hardware, circuits and the differences between the uplink and downlink counterparts are not modeled and are assumed to be tuned.

1.4 LITERATURE STUDY

There is a great amount of research currently going on in (multi-user-MIMO) (MU-MIMO) systems and how beamforming can be applied to these systems. The following two papers provide good overall knowledge of MU-MIMO and how far the research has come;

- In [2] the background and potentials of MU-MIMO and beamforming algorithms are described.
- A real-time physical model with 100 base station antennas has been built at Lund University at the department of Electrical and Information Technology. More information about this testbed is found in [3].

The intent with this thesis work is to create a simulation tool that is based on LTE where one should be able to implement and compare beamforming algorithms in a wide range of scenarios. The results of this work could then be used when developing LTE or for education purposes; for people that want to learn more about LTE and beamforming.

2 BACKGROUND

This section covers technical standards and basics of how LTE works to give the reader a better understanding of LTE before heading into more advanced topics. Only the parts that the authors deem necessary for a good understanding of this thesis are mentioned. The information mostly originates from 3rd Generation Partnership Project (3GPP) [4] which is an organization that collects and unites information from multiple telecommunications developers to form a standard. The books [5], [6] and [7] summarize and present information from 3GPP in a way that is easy to follow and these are the main sources of general information in the study.

2.1 UPLINK AND DOWNLINK

Transmission from user equipment (UE) to the base station is called uplink and transmission in the opposite direction is called downlink. The most notable difference between UL and DL is that they use different multiple-access techniques. Single carrier frequency division multiple access (SCFDMA) is used in the UL, which is good for the UE since it uses less power [5] than orthogonal frequency division multiple access (OFDMA) which is used in the DL. This is because in OFDMA the data is carried by a single subcarrier while in SCFDMA the data is carried by wider subcarriers. Thus the Peak to Average Power Ratio (PAPR) is lower for SCFDMA which makes the power amplification prior to transmission more efficient. With these multiple access techniques multiple streams of data to multiple users can be coded simultaneously in time.

There are two techniques to handle the DL and UL transmissions, namely frequency division duplex (FDD) and time division duplex (TDD). FDD is used to send UL and DL frames simultaneously using two separate frequency bands which means that data can be transmitted and received at the same time, increasing throughput. Another benefit with FDD is that it is easier to synchronize the packages since there are separate links for UL and DL. TDD on the other hand is just using one frequency band and the frames are divided in time instead, which means that the same channel is used for UL and DL transmissions and depending on the current flow in the network different UL/DL frame schemes can be used. This requires more precision in synchronization. In this thesis work TDD is used since the UL and DL channels are assumed to be reciprocal and almost stationary over a certain period of time which is beneficial for beamforming. More about beamforming is covered in Section 4.

There is a set of frequency bands that are assigned for LTE TDD and each of these bands is divided into channels with bandwidths according to Table 1. It is in one of these channels that the Matlab model operates in and the signals that are transmitted on the channel are described in the next section.

Channel Bandwidth	1.4 MHz	3 MHz	5 MHz	10 MHz	15 MHz	20 MHz
Subcarriers	72	180	300	600	900	1200
Resource Blocks	6	15	25	50	75	100

Table 1: Subcarriers and resource blocks as a function of the channel bandwidth, [5].

2.2 LTE RESOURCES

The largest unit in an LTE transmission is called a radio frame and it has two dimensions; time and frequency. Along the time axis it lasts for 10 ms. This radio frame is divided into 10 subframes which are 1 ms each which in turn is divided into two slots of 0.5 ms. There are 14 symbols in a subframe and 7 symbols in a slot. A symbol is the smallest unit in time and more about them is mentioned in Section 2.3. The radio frame and its subcomponents is shown in Fig. 1.

The length of the frequency axis depends on the channel BW, which is divided into numerous subcarriers which each has a width of 15 kHz. The number of subcarriers are therefore related to the BW and this relation is seen in Table 1.

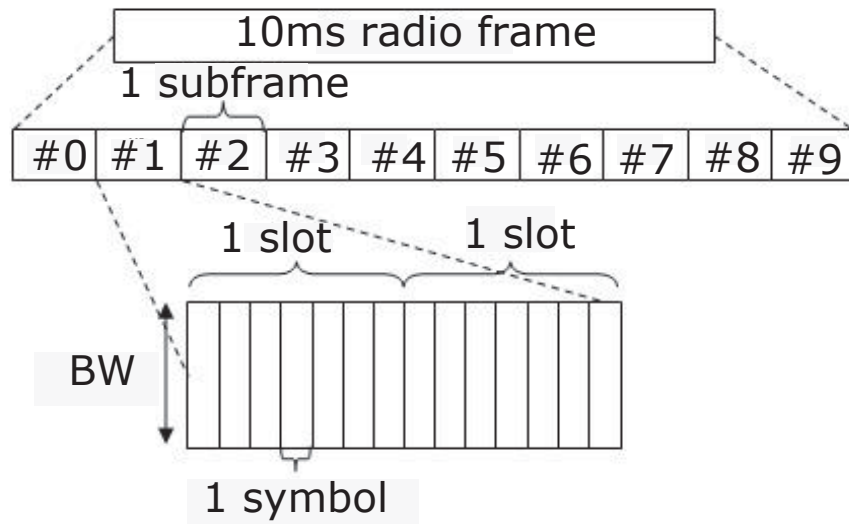


Figure 1: Illustration of a LTE radio frame and its subcomponents, [8].

If one multiplies the subcarrier frequency of 15 kHz with the number of subcarriers specified from the BW shown in Table 1. One can see that the subcarriers will not cover the entire BW, as the edges are left unused to act as a guard band to reduce interference from neighbouring channels.

If the time and frequency axes are combined, a grid will arise which is comprised of units called resource elements (RE) which occupy one subcarrier in frequency and one symbol in time. A larger grid containing 12 subcarriers and 7 symbols is called a resource block (RB). In the current implementation of LTE, two time-consecutive RBs, spanning 14 symbols is the smallest unit that can be transferred to one UE at a time. These blocks are assigned to each UE using a scheduler, however in this thesis scheduling is not used and each UE is assigned a static number of RBs. Fig. 2 shows an example of how a 1.4 MHz subframe with 72 subcarriers and 14 symbols could look like. Each color represents the allocation to one UE.

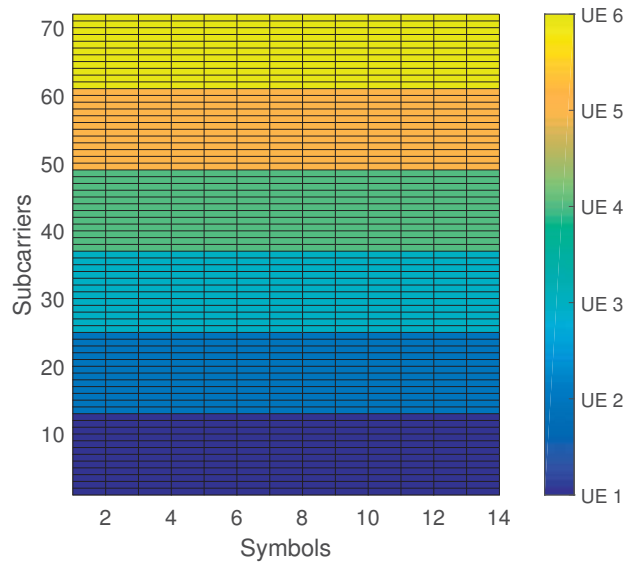


Figure 2: Six users in a 1.4 MHz bandwidth subframe.

2.3 TRANSMISSION OF USER DATA

The user data is transferred in two physical channels which are called physical uplink shared channel (PUSCH) for UL transmissions and physical downlink shared channel (PDSCH) for DL transmissions [5][7]. The channels have a set of resource elements allocated for data symbols, i.e. a set of indices in the time-frequency grid which contain the user data. The user data arrives as bits to the transmitter unit and is called a codeword (CW). The codeword can be further divided into either one or two streams of codewords, CW1 and CW2 as shown in Fig. 3 Before these codewords are transmitted from the physical antennas they are processed in a few steps. To keep the model simple, the steps in Fig. 3 are used which include symbol modulation, layer mapping, precoding, resource mapping and OFDMA or SCFDMA modulation. In a real system one would also like to include error detection which includes Cyclic redundancy check (CRC) insertion, code-block segmentation, turbo encoding, rate matching, code-block concatenation and scrambling as presteps to the ones shown in the figure. As mentioned earlier, error detection is not included to keep the signal processing of the transmitter and receiver chains simpler.

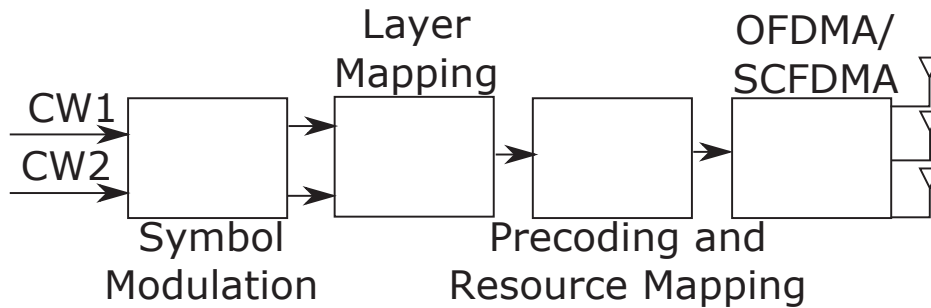


Figure 3: Transmitter chain [13].

Symbol modulation is the stage where the bits are converted from ones and zeros to a complex number. This is done by mapping a sequence of bits to a number in the complex plane. By giving a certain sequence of bits a certain amplitude and phase all combination of bits can be coded in sequence. In this project, four types of modulation techniques are used; QPSK, 16QAM, 64QAM and 256QAM which respectively maps 2, 4, 6 and 8 bits into a single symbol. Fig. 4 - Fig. 7 shows the resulting complex valued symbols after modulation with the four modulators. As seen in the figures, the more bits that are coded into a symbol the smaller the distance between each symbol will be. This means that modulation of a higher order will be more sensitive to noise compared to a modulation technique with a lower order. On the other hand, a higher order modulation technique will transfer more bits during the same time interval. Therefore the modulation should change with the channel conditions for optimal transmission. Note that the constellation diagrams are normalized such that the average power of the signal is equal to one.

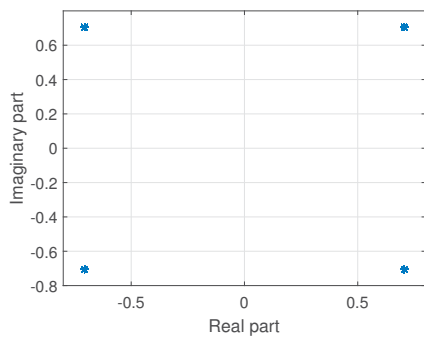


Figure 4: Constellation diagram QPSK.

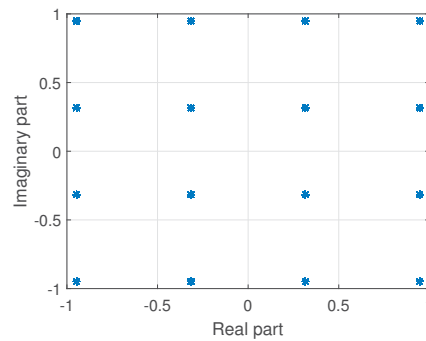


Figure 5: Constellation diagram 16QAM.

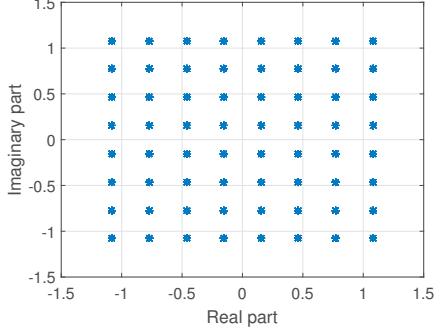


Figure 6: Constellation diagram 64QAM.

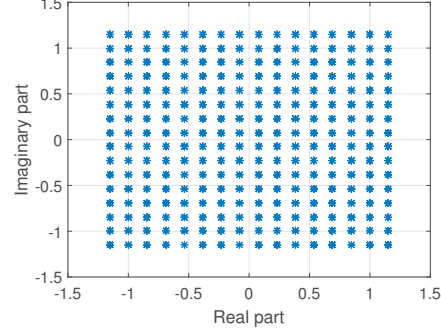


Figure 7: Constellation diagram 256QAM.

Layer mapping is done to assign each symbol in the stream of symbols to a specific layer. Layers in this context means the number of shared resources that are transmitted to the same user, and each layer must thus have orthogonal reference signals to be separated. Table 2 shows how the mapping depends on the number of codeword streams and the number of layers used, x^{layer} refers to a layer and $d^{codeword}$ refers to a codeword stream. M_{symb}^{layer} is the number of symbols for a specified layer. In this project two codewords are used when using more than one layer. The more layers that are used, the more data is transferred at the same time. Similar to modulation, the system is more sensitive to noise if it transmits more layers because it is more difficult to separate the layers. To have a system of full rank, which means that all the transmitted layers are successfully demodulated at the receiver, the system needs to have at least the same number of transmit and receiver antennas as the number of layers used.

Number of layers	Number of codewords	Codeword-to-layer mapping	$i = 0, \dots, M_{symb}^{layer} - 1$
1	1	$x^{(0)}(i) = d^{(0)}(i)$	$M_{symb}^{layer} = M_{symb}^0$
2	2	$x^{(0)}(i) = d^{(0)}(i)$ $x^{(1)}(i) = d^{(1)}(i)$	$M_{symb}^{layer} = M_{symb}^0 = M_{symb}^1$
3	2	$x^{(0)}(i) = d^{(0)}(i)$ $x^{(1)}(i) = d^{(1)}(2i)$ $x^{(2)}(i) = d^{(1)}(2i + 1)$	$M_{symb}^{layer} = M_{symb}^0 = M_{symb}^1/2$
4	2	$x^{(0)}(i) = d^{(0)}(2i)$ $x^{(1)}(i) = d^{(0)}(2i + 1)$ $x^{(2)}(i) = d^{(1)}(2i)$ $x^{(3)}(i) = d^{(1)}(2i + 1)$	$M_{symb}^{layer} = M_{symb}^0/2 = M_{symb}^1/2$

Table 2: Codeword-to-layer mapping [9].

The next two stages of coding are to precode the symbols of the layers with a set of weights and then to combine the layers and map them to the physical antennas. It is at this stage that beamforming is performed and each physical antenna will then

have its own weighted resource grid. More about the beamforming can be found in Section 4.

In the final step the grids are converted to a waveform using either OFDMA or SCFDMA for DL or UL transmissions respectively. Cyclic prefix insertion is an important part here [5]. In essence it is used to decrease the impact of the signal taking multiple paths with different delays. The effect of this delay spread is that signals arrive at different times. This means that two symbols with different time-index can arrive at the same time and interfere, which is called inter-symbol interference (ISI). When the receiver then samples the signal and does a fast Fourier transform (FFT) on the signal, it will contain a mix of frequencies from different symbols. This is a problem and to handle it a cyclic prefix is inserted to every symbol. The cyclic prefix itself is the last part of every symbol and the length depends on the type of prefix, normal or extended. A normal cyclic prefix will cover for delay spreads up to 1.5 km or about $5 \mu s$ and an extended prefix can handle delay spreads up to 5-10 km which is 16.7-33.3 μs . Thus all symbols that arrives within the delay spread, inside of the cyclic prefix, will be seen as the same symbol. The FFT computes the frequency content of the signal and the frequency content will not change with delayed components of the same signal. The last step of the modulation itself is to use an inverse Fourier transform (IFFT) on the complex-valued signals to translate them into the time domain. The signals are then transmitted on the wireless channel which is covered in Section 3, before they are received by the receiver chain explained in the next section.

2.4 RECEPTION OF USER DATA

The reception of data includes steps that are the inverse of the ones involved in the transmitter chain. Namely OFDMA- and SCFDMA-demodulation, layer demapping and symbol demodulation. Channel Estimation and Channel Equalization are also added to the chain and are very crucial in wireless transmission. The receiver chain that is used in the model in this thesis is shown in Fig. 8.

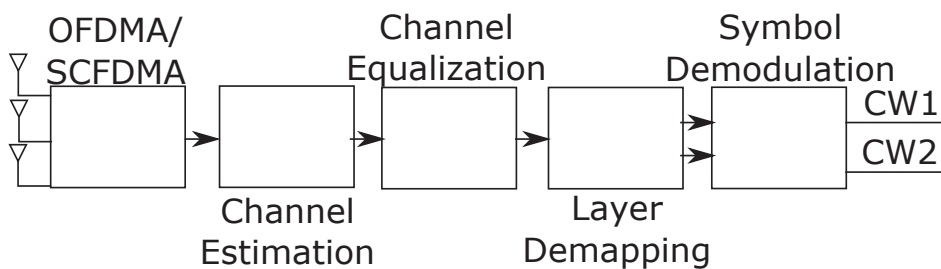


Figure 8: Receiver chain [13].

Channel estimation is needed because when signals are transmitted over a wireless channel, they lose their initial characteristics because of path loss, interference, fading and noise. For further explanation of these phenomena, see Section 3. Because of this, the signal will have a new amplitude and phase at the receiver. To compensate for this, known pilot symbols are placed at known indices in the resource grid and

more about pilot symbols is mentioned in Section 2.5. In this way the receiver can do channel estimation by comparing the received symbols with the known symbols. The symbols are spread across the grid depending on what transmission mode is used, the number of layers used and also if it is UL or DL transmission.

The channel estimate is computed according to the steps in [14]. First the channel estimate for all reference symbols is found using least squares. Then averaging is done on the estimated reference symbols with an averaging-window spanning both time and frequency domain to suppress the effect from noise. Interpolation is then performed between the pilot symbols to retrieve a channel estimate over the entire grid. It is done by finding the best fit of a line between the estimated and averaged symbols of each column in the grid. The line can for example be either linear or cubic. The unknown symbols are then found from the indices of the fitted line and all of the lines are put together to a grid. Virtual pilot symbols may also be inserted outside of the grid to increase the performance of the interpolation at the grid edges. These virtual pilots are found from a grid that is formed from the cross product of the original pilots closest to the virtual pilot that you wish to generate.

Channel equalization is used to retrieve the user data from the channel estimate. This is simply the inverse channel estimate multiplied with the received symbols to remove the channel impact. There are two well known ways of doing this, zero-forcing (ZF) and minimum mean-squared error (MMSE). The difference between the two methods is that MMSE uses the channel noise estimate while the ZF does not. The effect of this is that MMSE gives an equal or better estimate compared to ZF over the entire SNR range [10].

2.5 REFERENCE SIGNALS

This thesis is focusing on transmission mode (TM) 9 and multilayer transmissions and therefore the UE specific reference signal is used, it is also known as the demodulation reference signal (DM-RS). DM-RS generation differs between UL and DL both in signal generation and in grid indices [9, sections 5.5 and 6.10.3]. The idea with the DM-RS signal is that both the transmitter and receiver should be able to generate the same sequence based on a number of parameters and thus be able to estimate the channel. Because both transmitter and receiver knows what the sequence should look like, they can estimate how the channel has affected the signal. In the uplink, the signal is generated from a Zadoff-Chu sequence, which has the good properties that it has a constant amplitude and can be sequentially shifted for orthogonality between cells [11]. Orthogonal cover codes (OCC)s are used to achieve orthogonality between layers by multiplying them with one Zadoff-Chu sequence to get a sequence for each layer. Creating orthogonality in this way is referred to as code division multiplexing (CDM). The OCCs used in this thesis are

$$\begin{aligned} \mathbf{OCC}(\lambda) &= e^{i\alpha(\lambda)\mathbf{L}}, \quad \mathbf{L} = [0, 1, 2, \dots, k] \\ \alpha(\lambda) &= (0 \quad \pi \quad -\pi/2 \quad \pi/2), \end{aligned} \tag{1}$$

where $\mathbf{OCC}(\lambda)$ is the OCC for layer λ and with the phase shift α , the sequences will be orthogonal to each other, i.e. the dot product between the sequences is equal

to zero [12]. The sequence length k depends on the number of subcarriers [15]. To get a good estimate of the entire uplink channel BW for all UEs, the UE pilots are sequentially allocated in the grid [3]. The resulting combined pattern of six UEs in a 1.4MHz BW channel is shown in Fig. 9, symbol columns 4 and 11 are the pilot symbols and the rest are user data. The data resources are shared among all UEs and the base station will be able to find the symbol for each individual UE since it has the channel estimate of the entire channel for each UE. When transmission is done in the model, each UE just transmits its own pilot symbols and leaves the rest empty, the figure is just as a visual aid.

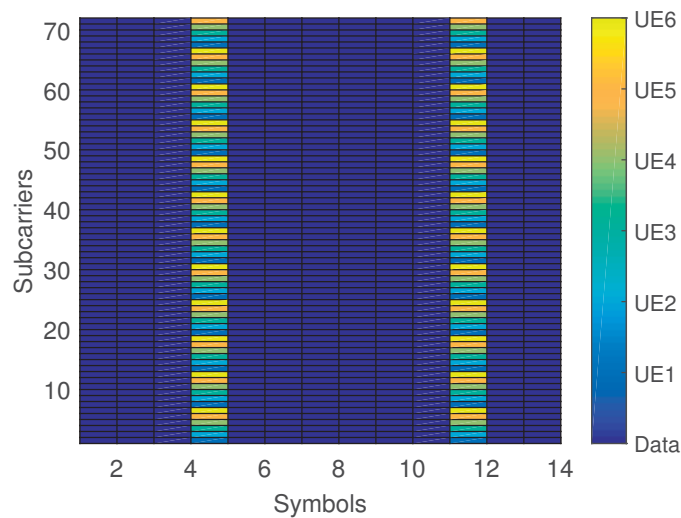


Figure 9: User allocation for six users in a 1.4 MHz bandwidth UL subframe.

According to LTE terminology, the downlink transmission is done on port 7 to 14 and the number of ports used is equal to the amount of layers to be transmitted [6]. Orthogonality between layers is obtained by using a mixture of frequency division multiplexing (FDM) and CDM [5]. FDM is done by transmitting on different subcarriers; Ports 7,8,11 and 13 are transmitting on the same indices and ports 9, 10, 12 and 14 are shifted downwards with one subcarrier compared to these and thus FDM is obtained. Within these two groups of ports CDM is used to get orthogonal sequences.

3 WIRELESS CHANNEL

This section aims to describe all parts that comprise the channel model in as much detail as needed to piece together the complete model. Reasons for choosing the models used in this work are brought up and possible alternatives are presented, which should serve as a starting point for finding possible flaws in the model and subsequently improving upon it.

3.1 CHANNEL MODEL

3.1.1 FADING MODEL

The wireless channel between user and base station is typically modeled using two different probability distributions, depending on whether the user has a direct line-of-sight to the base station or not. If there is a direct line-of-sight a Rician distribution is used to model the complex-valued filter coefficients used to represent the channel and if not, a Rayleigh distribution is used. Since one can generally not assume there to be a line-of-sight between base station and UE, the distribution used to model the channel is a Rayleigh distribution, which has the probability density function

$$p_R(r) = \frac{2r}{\Omega} e^{-\frac{r^2}{\Omega}}, \quad r \geq 0 \quad \text{where } \Omega = E(R^2), \quad (2)$$

R is the random variable r is the value for which the probability is evaluated and $E(R^2)$ is the variance of R . The Rayleigh distributed variables are generated using a method that creates a sum of sinusoids with independent uniformly distributed phase and amplitude as well as a frequency shift factor. There are several known methods of generating these sinusoids and the one used in this thesis has been shown to exhibit good statistical properties and was presented in [16]. As opposed to other similar methods such as Jakes', the sum of sinusoids is properly stochastic in its nature and different generated paths are mutually uncorrelated [16]. Another property of this method is that it is very easy to generate exactly as many samples as needed. The sum of sinusoids method is outlined in (3). This method converges quickly to the Rayleigh distribution, so the computational cost can be kept low with a value of M around 10 [16].

$$\begin{aligned} X(t) &= X_c(t) + jX_s(t) \\ X_c(t) &= \frac{2}{\sqrt{M}} \sum_{n=1}^M \cos(\psi_n) \cos(\omega_d t \cos(\alpha_n) + \phi) \\ X_s(t) &= \frac{2}{\sqrt{M}} \sum_{n=1}^M \sin(\psi_n) \cos(\omega_d t \cos(\alpha_n) + \phi) \\ \text{with } \alpha_n &= \frac{2\pi n - \pi + \theta}{4M}, \quad n = 1, 2, \dots, M \end{aligned} \quad (3)$$

where M is the number of sinusoids to sum, ψ_n , ϕ and θ are uniformly distributed on $[-\pi, \pi) \forall n$, and ω_n is the maximum Doppler frequency.

3.1.2 TIME CORRELATION

Since the user is usually moving, the channel will also change over time, usually causing the received signal strength to deteriorate at random intervals. This is because the received signal is a sum of all the different reflections of the sent signal that propagates via different paths provided by the environment. At some points these reflected signals may interfere destructively, while at other points they boost the signal strength. This phenomenon is called multipath fading. The rate at which the channel is expected to experience a change in amplitude corresponds to how fast the user is moving and is characterized by the Doppler spectrum related to that velocity. The Doppler spectrum causes a temporal correlation in the channel, causing subsequent samples to be correlated. This is also modeled in the Rayleigh model presented by (3).

In the LTE standard [18], the number of most significant signal paths and their respective relative tap delays and losses are typically determined into three different scenarios; "Extended Pedestrian A" (EPA), "Extended Vehicular A" (EVA) and "Extended Typical Urban" (ETU) as shown in Table 3.

Profile	Tap Delays (ns)
EPA	[0 30 70 90 110 190 410]
EVA	[0 30 150 310 370 710 1090 1730 2510]
ETU	[0 50 120 200 230 500 1600 2300 5000]
Profile	Relative Power (dB)
EPA	[0.0 -1.0 -2.0 -3.0 -8.0 -17.2 -20.8]
EVA	[0.0 -1.5 -1.4 -3.6 -0.6 -9.1 -7.0 -12.0 -16.9]
ETU	[-1.0 -1.0 -1.0 0.0 0.0 0.0 -3.0 -5.0 -7.0]
Profile	Max. Doppler Frequency (Hz)
EPA	5
EVA	5 or 70
ETU	70 or 300

Table 3: Parameters for the different delay profiles specified in LTE [18].

For each of these paths, a complex-valued Rayleigh distributed sequence is generated as outlined in Section 3.1.1. Each sequence then acts as the time-varying envelope with which the signal is filtered. The absolute value of envelopes with different Doppler spectra is shown in Fig. 10 and 11.

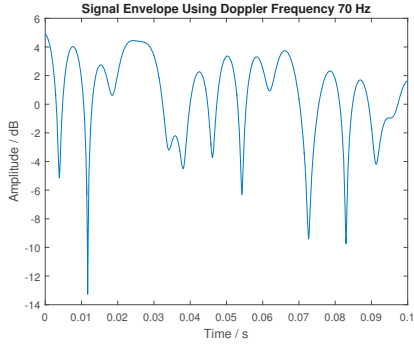


Figure 10: Signal envelope for 0.1 seconds with a maximum Doppler frequency of 70 Hz.

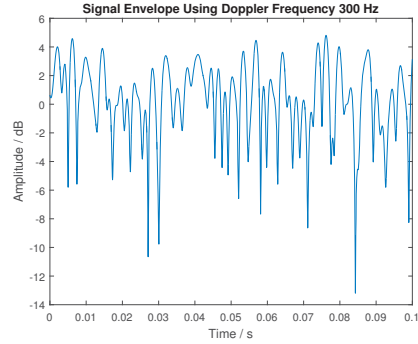


Figure 11: Signal envelope for 0.1 seconds with a maximum Doppler frequency of 300 Hz.

3.1.3 FILTER STRUCTURE & SPATIAL CORRELATION

The MIMO channel for one of k users is shown in Fig. 12 with each user having j antennas. There is m base station antennas and each channel $\mathbf{H}_{k,j,m}$ consists of n paths, each path having a delay τ_n and an instantaneous gain $h_n(t)$. This defines the filter taps for a time varying FIR filter through which the signal is subsequently filtered.

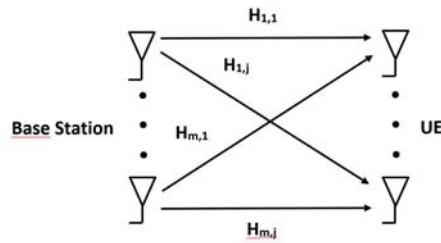


Figure 12: MIMO channel between one user and base station.

The filter structure is shown in Fig. 13 and is repeated for each transmitter-receiver antenna pair.

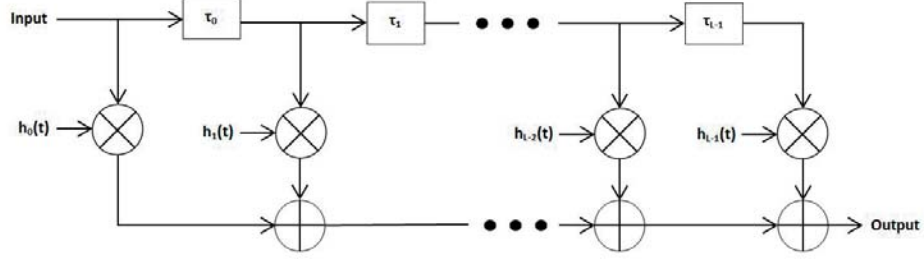


Figure 13: Time-varying FIR filter structure used for the channel.

Thus far in the model, the channel for each antenna pair is modeled as independent. However, as the antennas at the transmitting and receiving ends are placed very closely, a spatial correlation between the channels of the antennas arises. This is modeled using a Kronecker model and is also standardized in LTE with regards to the level of correlation, being divided into low, medium and high [18]. Examples of the correlation matrices and their values can be seen in (4), (5) and Table 4 respectively for the 2x2 and 4x4 MIMO cases. The transmitter and receiver correlation is assumed to be independent and separable using a Kronecker model [19]

$$\mathbf{R}_{\text{ue}} = \begin{pmatrix} 1 & \beta \\ \beta^* & 1 \end{pmatrix}, \quad \mathbf{R}_{\text{enb}} = \begin{pmatrix} 1 & \alpha \\ \alpha^* & 1 \end{pmatrix} \quad (4)$$

$$\mathbf{R}_{\text{ue}} = \begin{pmatrix} 1 & \beta^{1/9} & \beta^{4/9} & \beta \\ \beta^{1/9*} & 1 & \beta^{1/9} & \beta^{4/9} \\ \beta^{4/9*} & \beta^{1/9*} & 1 & \beta^{1/9} \\ \beta^* & \beta^{4/9*} & \beta^{1/9*} & 1 \end{pmatrix}, \quad \mathbf{R}_{\text{enb}} = \begin{pmatrix} 1 & \alpha^{1/9} & \alpha^{4/9} & \alpha \\ \alpha^{1/9*} & 1 & \alpha^{1/9} & \alpha^{4/9} \\ \alpha^{4/9*} & \alpha^{1/9*} & 1 & \alpha^{1/9} \\ \alpha^* & \alpha^{4/9*} & \alpha^{1/9*} & 1 \end{pmatrix} \quad (5)$$

$$\mathbf{H} = \mathbf{R}_{\text{r}}^{1/2} \mathbf{H}_{\text{w}} (\mathbf{R}_{\text{t}}^{1/2})^T, \quad (6)$$

where α and β are chosen from Table 4. \mathbf{R}_{r} is the receiver correlation matrix and \mathbf{R}_{t} is the transmitter correlation matrix, which both depend on whether UL or DL transmission is modeled and are chosen as \mathbf{R}_{ue} or \mathbf{R}_{enb} . This model could hold since the user and base station are very far apart and the channel is comprised of Rayleigh distributed independent and identically distributed (i.i.d) variables [19]. While this is widely used in present LTE simulations, more research into the correlation of MIMO systems is warranted, especially as the number of antennas increase. Essentially, the Kronecker model could underestimate the correlation for systems larger than 4x4 [19]. Realistically, one would expect the spatial correlation to depend on the configuration of the antenna array, i.e. how the antennas are arranged as well as the directivity of the individual antennas [20].

Correlation:	Low	Medium	High
α :	0	0.3	0.9
β :	0	0.9	0.9

Table 4: Correlation levels specified in LTE [18].

3.1.4 LARGE SCALE FADING

In addition to the fast-changing multipath fading determined by the Doppler shift, there is a large scale fading effect as well. This effect stems from the fact that while moving, a user can end up with a better or worse signal because of for example buildings, which are said to shadow the user. This fading is much slower-changing than the multipath fading and follows a lognormal distribution [21]

$$pdf_F(F) = \frac{20/\ln(10)}{F\sigma_F\sqrt{2\pi}} e^{-\frac{(20\log_{10}(F)-\mu_{dB})^2}{2\sigma_F^2}}, \quad (7)$$

where σ_F is the standard deviation (SD) of F and μ_{dB} is the mean of F in dB. The standard deviation of F is in the range of 4-10 dB [21] and this fading is centered around zero when generated. The large scale fading is then superimposed on the time-varying filter taps for each user independently. Since this is an effect of the user moving, the large scale fading will be correlated through time just as the multipath fading.

3.1.5 PATH LOSS

On top of the multipath fading and large scale fading effects, there is also a path loss attributed to the wireless channel. Assuming that the transmission is done in a no line-of-sight urban area the WINNER path loss model [22] is given by

$$PL_{dB} = 23.5\log_{10}(d) + 57 + 23\log_{10}\left(\frac{f_c}{5}\right), \quad (8)$$

where f_c is the carrier frequency in GHz ($2 \text{ GHz} < f_c < 5 \text{ GHz}$) and d is the distance in meters between the receiver and transmitter ($30 \text{ m} < d < 5 \text{ km}$). Furthermore the height of the base station and UEs are assumed to be 25 m and 1.5 m respectively. (8) in conjunction with the antenna gains is called the Friis transmission equation and is given by

$$P_r - P_t = G_t + G_r - PL_{dB}. \quad (9)$$

This represents the difference between received and transmitted power during transmission from one antenna to another, including antenna gains G_t and G_r .

3.2 UPLINK AND DOWNLINK RECIPROCITY

Since the duplexing mode used is TDD, the channel is highly correlated, if not constant between frames and particularly between UL and DL transmission. This is

because the same frequencies are used to transmit both in the UL and DL, and thus frequency dependent effects of the channel are similar between UL and DL. The most important element that changes is the fading, which is determined by the Doppler frequency and temporal correlation by advancing the channel one subframe in time. The other element that changes is the processing chain between transmitter and receiver, importantly the amplifier used at the base station which is a high-power amplifier contra the UE, which uses a low-power amplifier. Because they use different amplifiers, the perceived channel will differ between UL and DL. This is currently not modeled as explained in Section 1.3.

3.3 NOISE

The background noise used in the model is a simple well known thermal noise model [23] given by

$$v_n^2 = 4k_B TR\Delta f, \quad (10)$$

where v_n^2 is the variance of the noise in Volts, k_B is the Boltzmann constant, T is the temperature in Kelvin, R is the resistance of the load in Ohm and Δf is the bandwidth of the signal in Hz. The temperature is chosen as 300 K, "room temperature" and realistically will only vary at most ± 30 K. The load resistance is chosen as the nominal impedance for radio systems; 50 Ohm, and the bandwidth can be selected from the different transmission standards within LTE [4] ranging from 1.4 MHz to 20 MHz as in Table 1.

3.4 COHERENCE TIME

As the channel changes over time, the beamforming will have to adapt to these changes in order to keep good performance. A measure of how quickly the channel is changing is the coherence time [24]

$$T_c = \sqrt{\frac{9}{16\pi f_d^2}} \quad (11)$$

where f_d is the maximum Doppler frequency. The coherence time tells us approximately how long the channel will be time-invariant. This can be used to approximate how long the beamforming weights will be valid for.

4 DOWNLINK BEAMFORMING

This section starts by describing some basics with beamforming and how it works from a physical point of view and then continues with beamforming algorithms and how they are implemented in the LTE model.

When two waves propagate in free space it is known from basic physics [25] that they interfere with each other if they are at the same position at the same time. If this happens the amplitudes of the two waves are summed up and the interference can be constructive, destructive or something in between. It is considered constructive when the waves have the same phase and the amplitude will then become higher than that of one single wave. Conversely, destructive interference happens when the waves are phase-shifted such that the total amplitude of the two waves becomes less than that of a single wave. Interference is used in practice by building an antenna array with many antennas and transmit phase-shifted versions of the same signal from each antenna in the array. The total beam of all antennas will then interfere constructively in some directions and destructively in others. If information about the channel between the UEs and base station is known, the beamforming weight for each antenna can be found such that the total beam can be steered towards the UEs. There are many ways of doing this, but in this thesis the focus will be on known linear precoding techniques that either maximizes the signal to noise ratio (SNR) or the signal to interference and noise ratio (SINR) at each user in the system as in

$$\mathbf{Y} = \mathbf{H}_{\text{DL}}\mathbf{W}\mathbf{X} + \mathbf{n}, \quad (12)$$

where \mathbf{W} is the beamforming weighting matrix, \mathbf{X} is the signals from all users, \mathbf{n} is i.i.d Gaussian noise, \mathbf{Y} is a matrix with users and \mathbf{H}_{DL} is the downlink channel matrix with the instantaneous gain and delay from each multipath between the K single antenna users and the M base station antennas. This channel matrix is further defined as

$$\mathbf{H}_{\text{DL}} = \begin{pmatrix} \mathbf{h}_{\text{DL}1,1}(\mathbf{s}) & \cdots & \mathbf{h}_{\text{DL}1,M}(\mathbf{s}) \\ \vdots & \ddots & \vdots \\ \mathbf{h}_{\text{DL}K,1}(\mathbf{s}) & \cdots & \mathbf{h}_{\text{DL}K,M}(\mathbf{s}) \end{pmatrix}. \quad (13)$$

Each element $\mathbf{h}_{\text{DL}}(\mathbf{s})$ in \mathbf{H}_{DL} is the instantaneous downlink channel amplitude and phase for the symbol located at index \mathbf{s} in the resource grid as in

$$\mathbf{h}_{\text{DL}}(\mathbf{s}) = \begin{pmatrix} h_{DL1,1} & \cdots & h_{DL1,14} \\ \vdots & \ddots & \vdots \\ h_{DL1200,1} & \cdots & h_{DL1200,14} \end{pmatrix}, \quad (14)$$

where $\mathbf{s} = [s_1, s_2]$ and $s_1 = 1, 2, \dots, 1200$, $s_2 = 1, 2, \dots, 14$ for a 20MHz BW channel with 1200 subcarriers and 14 symbols. The idea is to loop through all symbols and find the beamforming weight \mathbf{W} for one symbol index at a time and then to weight this

symbol from all users $\mathbf{X}(\mathbf{s})$ to all antennas $\mathbf{A}(\mathbf{s})$ using

$$\begin{pmatrix} \mathbf{A}_1(\mathbf{s}) \\ \vdots \\ \mathbf{A}_M(\mathbf{s}) \end{pmatrix} = \begin{pmatrix} \mathbf{W}_{1,1}(\mathbf{s}) & \cdots & \mathbf{W}_{1,K}(\mathbf{s}) \\ \vdots & \ddots & \vdots \\ \mathbf{W}_{M,1}(\mathbf{s}) & \cdots & \mathbf{W}_{M,K}(\mathbf{s}) \end{pmatrix} \begin{pmatrix} \mathbf{X}_1(\mathbf{s}) \\ \vdots \\ \mathbf{X}_K(\mathbf{s}) \end{pmatrix}, \quad (15)$$

where $\mathbf{X}(\mathbf{s})$ and $\mathbf{A}(\mathbf{s})$ is the same size as one resource grid and thus has the same size as $\mathbf{h}_{\text{DL}}(\mathbf{s})$. The weighted signals from all UEs are then transmitted over the channel according to

$$\begin{pmatrix} \mathbf{Y}_1(\mathbf{s}) \\ \vdots \\ \mathbf{Y}_K(\mathbf{s}) \end{pmatrix} = \begin{pmatrix} \mathbf{h}_{\text{DL}1,1}(\mathbf{s}) & \cdots & \mathbf{h}_{\text{DL}1,M}(\mathbf{s}) \\ \vdots & \ddots & \vdots \\ \mathbf{h}_{\text{DL}K,1}(\mathbf{s}) & \cdots & \mathbf{h}_{\text{DL}K,M}(\mathbf{s}) \end{pmatrix} \begin{pmatrix} \mathbf{A}_1(\mathbf{s}) \\ \vdots \\ \mathbf{A}_M(\mathbf{s}) \end{pmatrix} \quad (16)$$

Multiple layers can be sent to each UE if the UEs are equipped with one antenna for each layer, resulting in a total of N antennas and layers. By introducing this into the equations, (15) and (16) are extended to (17) and (18) respectively as

$$\begin{pmatrix} \mathbf{A}_1(\mathbf{s}) \\ \vdots \\ \mathbf{A}_M(\mathbf{s}) \end{pmatrix} = \begin{pmatrix} \mathbf{W}_{1,1,1}(\mathbf{s}) & \cdots & \mathbf{W}_{1,1,N}(\mathbf{s}) & \cdots & \mathbf{W}_{1,K,1}(\mathbf{s}) & \cdots & \mathbf{W}_{1,K,N}(\mathbf{s}) \\ \vdots & \ddots & \vdots & \ddots & \vdots & \ddots & \vdots \\ \mathbf{W}_{M,1,1}(\mathbf{s}) & \cdots & \mathbf{W}_{M,1,N}(\mathbf{s}) & \cdots & \mathbf{W}_{M,K,1}(\mathbf{s}) & \cdots & \mathbf{W}_{M,K,N}(\mathbf{s}) \end{pmatrix} \begin{pmatrix} \mathbf{X}_{1,1}(\mathbf{s}) \\ \vdots \\ \mathbf{X}_{1,N}(\mathbf{s}) \\ \vdots \\ \mathbf{X}_{K,1}(\mathbf{s}) \\ \vdots \\ \mathbf{X}_{K,N}(\mathbf{s}) \end{pmatrix} \quad (17)$$

$$\begin{pmatrix} \mathbf{Y}_{1,1}(\mathbf{s}) \\ \vdots \\ \mathbf{Y}_{1,N}(\mathbf{s}) \\ \vdots \\ \mathbf{Y}_{K,1}(\mathbf{s}) \\ \vdots \\ \mathbf{Y}_{K,N}(\mathbf{s}) \end{pmatrix} = \begin{pmatrix} \mathbf{h}_{\text{DL}1,1,1}(\mathbf{s}) & \cdots & \mathbf{h}_{\text{DL}1,1,M}(\mathbf{s}) \\ \vdots & \ddots & \vdots \\ \mathbf{h}_{\text{DL}1,N,1}(\mathbf{s}) & \cdots & \mathbf{h}_{\text{DL}1,N,M}(\mathbf{s}) \\ \vdots & \ddots & \vdots \\ \mathbf{h}_{\text{DL}K,1,1}(\mathbf{s}) & \cdots & \mathbf{h}_{\text{DL}K,1,M}(\mathbf{s}) \\ \vdots & \ddots & \vdots \\ \mathbf{h}_{\text{DL}K,N,1}(\mathbf{s}) & \cdots & \mathbf{h}_{\text{DL}K,N,M}(\mathbf{s}) \end{pmatrix} \begin{pmatrix} \mathbf{A}_1(\mathbf{s}) \\ \vdots \\ \mathbf{A}_M(\mathbf{s}) \end{pmatrix} \quad (18)$$

Three known beamforming algorithms are used in this work to find the beamforming weights \mathbf{W} and these algorithms are described in the next three subsections. To transmit in the opposite direction, the rows and columns of the channel matrix must be swapped to keep the same channel between receiver and transmitter. Thus

the algorithms uses the transpose of the uplink channel estimate to produce the downlink channel estimate, which we refer to as

$$\mathbf{H} = \begin{pmatrix} \mathbf{h}_{\text{UL},1}(\mathbf{s}) & \cdots & \mathbf{h}_{\text{UL},M,1}(\mathbf{s}) \\ \vdots & \ddots & \vdots \\ \mathbf{h}_{\text{UL},1,K}(\mathbf{s}) & \cdots & \mathbf{h}_{\text{UL},M,K}(\mathbf{s}) \end{pmatrix}^T \quad (19)$$

where $\mathbf{h}_{\text{UL}}(\mathbf{s})$ is the uplink channel estimate for each symbol \mathbf{s} and has the same size as $\mathbf{h}_{\text{DL}}(\mathbf{s})$ in (14).

4.1 MAXIMUM RATIO TRANSMISSION

As explained in [26], maximum ratio transmission (MRT) maximizes the SNR for each user. This algorithm has very low complexity as it is the Hermitian of the channel \mathbf{H} , i.e. the conjugate-transpose of the channel and the beamforming weights are chosen according to

$$\mathbf{W}_{\text{MRT}} = \mathbf{H}^H. \quad (20)$$

The cost of the low complexity is that the system is sensitive to inter-user interference which increases with the number of UEs in the system. The interference also originates from channel correlation and white noise and this reduces the orthogonality of the system which in turn leads to a lower throughput.

4.2 ZERO-FORCING

The well known ZF algorithm maximizes the signal to interference and noise ratio (SINR) of the system and it has been explained in previous work [26], [27] and [28]. Some good properties of this algorithm are that it cancels interference between users and is straight forward to implement since the beamforming weights are the pseudo-inverse of the channel. A drawback with this algorithm compared to MRT is the increased complexity due to inversion calculations. One condition for the ZF to be a well defined problem is that the number of base station antennas must be at least the total number of all user antennas as stated in

$$M \geq KN, \quad (21)$$

where, once more, M is the number of base station antennas, K the number of UEs and N the number of antennas per UE. The beamforming weights \mathbf{W} are then calculated as the pseudo-inverse of the channel matrix \mathbf{H} ;

$$\mathbf{W}_{\text{ZF}} = \mathbf{H}^H (\mathbf{H}\mathbf{H}^H)^{-1}. \quad (22)$$

4.3 REGULARIZED ZERO-FORCING

The ZF algorithm itself does not include any noise model in the weight estimation, which leads to the regularized zero forcing (RZF). The RZF algorithm is

$$\mathbf{W}_{\text{RZF}} = \mathbf{H}^H (\mathbf{H}\mathbf{H}^H + \alpha \mathbf{I}_M)^{-1}, \quad (23)$$

and as seen here RZF is an extension to ZF where α is to be determined to reduce the effect of noise in the system. The solution to RZF becomes the MMSE solution when $\alpha = \frac{K\sigma_h^2}{p_{dl}}$, where σ_h^2 is the channel noise variance and p_{dl} is the downlink power [26]. If α equals zero, which means low SNR, RZF becomes ZF and as $\alpha \rightarrow \infty$ RZF normalized by α converges to the MRT solution.

4.4 MASSIVE MIMO

There are theoretical benefits of massive MIMO in the form of

$$\frac{1}{M} \mathbf{H}\mathbf{H}^H \rightarrow \sigma_h^2 \mathbf{I} \quad \text{as } M \rightarrow \infty. \quad (24)$$

This means that the beamforming algorithms is able to remove most of the inter-user interference when the number of base station antennas is high enough [26]. For the MRT algorithm this result is very satisfactory, as it means that MRT can get the same performance as the ZF algorithms with less computational complexity when using many base station antennas.

4.5 POWER ALLOCATION

As the beamforming weights \mathbf{W} are found as described previously, they are expected to be quite large and therefore introduce a large gain when used directly. This is because of the channel inversion, especially when path loss is modeled, which is in the range of 100 dB. Because of power constraints, the weights also need to be power limited. Two normalizations techniques are considered; equal transmit power (ETP) and equal receive power (ERP). ETP has a higher sum-power and sum-rate and it is therefore chosen to normalize the beamforming weights [29]. The total power budget of the two normalization techniques equals the number of UEs. ERP normalizes the power so that the received power of the UEs will be equal while ETP normalizes the power of all transmitter antennas to the number of UEs. In other words, for ETP the base station antennas will share the power budget that is equal to the number of UEs in the model. Subsequently for a constant number of UEs the M transmitter antennas will always have the same total power. The ETP normalization is defined as

$$\begin{aligned} \mathbf{W} &= (\mathbf{w}_1 \quad \mathbf{w}_2 \quad \cdots \quad \mathbf{w}_K) \\ c_i &= \mathbf{w}_i^H \mathbf{w}_i, \quad i = 1, 2, \dots, K \\ \mathbf{W}_{\text{ETP}} &= \left(\frac{\mathbf{w}_1}{\sqrt{c_1}} \quad \cdots \quad \frac{\mathbf{w}_K}{\sqrt{c_K}} \right) \end{aligned} \quad (25)$$

where \mathbf{w} are the columns of \mathbf{W} [29]. This normalization means that the total power is 0 dBm before amplifying. This is useful since dBm is a power relating to 1 mW

and by relating the signal power to a physical quantity, the signal can be amplified such that all the available power is fully utilized. This means a total power across all base station antennas of 46 dBm and a total of 23 dBm for each UE [18]. The power allocated to each antenna could then be decided through different allocation schemes. One such scheme is to allocate different users different power, which can be further specified whether the goal is equal throughput to all users, or maximizing total throughput. In the present model however, a more heuristic scheme of dividing the power equally among the base station antennas is used.

5 MODELING USING LTE SYSTEM TOOLBOX IN MATLAB

5.1 INTERFACE

The Matlab model is constructed as a graphical user interface (GUI) to make testing and comparison with different setups easier due to all the parameters that are included in an LTE model. Even though the model is made to be as simple as possible and yet have the necessary functions, there are a lot of user parameters that can be set as shown in Fig. 14. On the left hand side of the GUI one can see all parameters that can be changed in the model and they are divided into two groups; channel and link parameters. The name of the parameter reveals most of its functionality but more precisely how they affect the underlying model is described in the following sections. Other than the user parameters there are also plots that show results from simulations and buttons for channel creation and frame transmission.

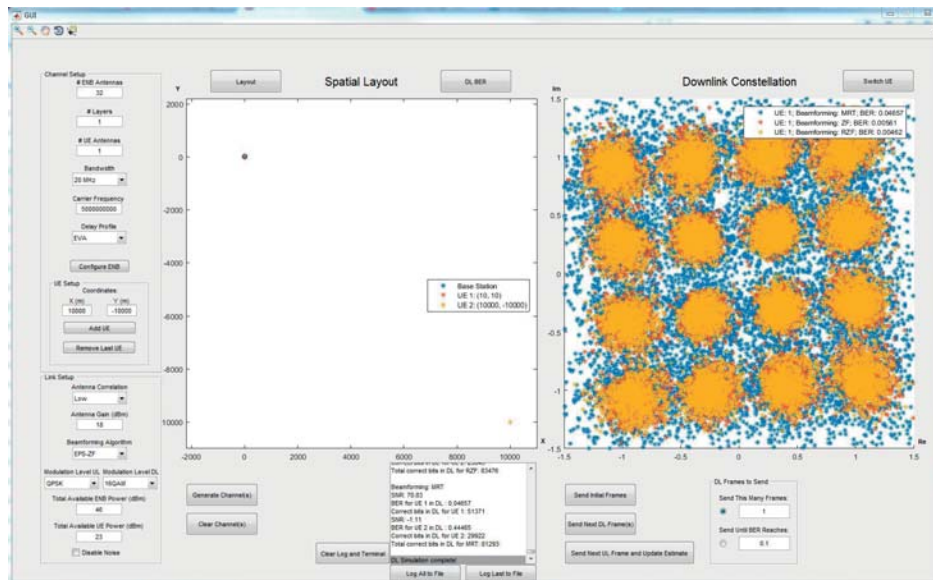


Figure 14: GUI.

The following list contains a summary of what the model supports to get an overview of its functionality;

- TDD transmission in UL and DL
- Scalable in terms of number of base station antennas and UEs
- Transmit 1-4 Layers to each UE
- LTE BWs of 1.4-20 MHz
- Four delay profiles; EPA, EVA, ETU and custom input

- Four modulation levels in DL; QPSK, 16QAM, 64QAM and 256QAM
- MRT, ZF and RZF beamforming
- Can transmit consecutive UL/DL frames on a time correlated channel
- Performance is presented in a constellation diagram and as bit error rate (BER) from frame to frame

5.1.1 CHANNEL SETUP

All parameters within this group basically have to do with the channel as stated in the title. The "#ENB Antennas" setting is simply the number of base station antennas to be used in the simulation and they are plotted in the Spatial Layout plot together with the number of UEs that are added from the add UE panel. The distances are in meters and the plot is there to remind the user of how many users he or she has added. The carrier frequency sets the spacing between the base station antennas and affects the path loss in the model. The bandwidth chooses the amount of subcarriers that are used according to Table 1 and under the button "Configure ENB" the length of the channel in time is decided as the total number of subframes. This is to ensure that the frames are time correlated and continuous. Layers determine the number of shared resources that should be transmitted to each UE and each UE should also be equipped with at least that number of antennas for a sufficient transmission. Finally the delay profile is chosen as either EPA, EVA, ETU or as a custom made model. EPA is the simplest model as it models a pedestrian and ETU is the most complex, modeling long distances in urban terrain.

When all of the parameters are set, the channels are created by pressing the button "Generate Channel(s)". The channels are generated as described in Sections 3.1 and 5.3, and the channels can also be cleared to the default settings by pressing "Clear Channel(s)". Worth mentioning is that the generated channels can be used multiple times with different link setups. This is implemented since channel generation can be a time consuming part of the simulation when simulating a high BW with many users and base station antennas. This way many different settings can be tested without having to regenerate the channels.

5.1.2 LINK SETUP AND TRANSMISSION

We start from the top of the link setup with "Antenna Correlation". This is the correlation between the UE antennas and the correlation between the ENB antennas, and can be chosen as low, medium, or high according to Table 4. The next option is a list menu to choose between the implemented downlink beamforming algorithms which are described in Section 4. Further, the modulation level can be set for the UL and DL respectively and determines the amount of data to transmit as mentioned in Section 2.3. There is QPSK, 16QAM and 64QAM in both directions and there is also 256QAM in the DL. The two next parameters "ENB Power" and "UE Power" decides how much total power is available to the base station and UEs respectively during transmission.

Subframes are generated and transmitted with the buttons located in the bottom right of the GUI window. "Send Initial Frames" transmits one uplink frame to get an estimate of the channel and then it transmits one downlink frame that is weighted with the beamforming weights found using the uplink estimate. The received downlink constellation at the UE will be shown in the right plot and if there are multiple UEs in the model the button "Switch UE" will toggle between the constellation diagrams of the different UEs. The user can choose to send consecutive downlink frames to see how the performance of the beamforming algorithm changes with time with "Send Next DL Frame(s)". This can also be illustrated in the left plot; if the "DL BER" button is pressed a plot of the BER as a function of time for one UE will be shown. The "Switch UE" button will also toggle between the BER plots. If one wishes to return to the spatial layout the button "Layout" can be used, and finally if one wishes to update the beamforming weights, the button "Send Next UL Frame and Update Estimate" will do as stated in the button text.

There is also a terminal that prints the SNR, BER and total transmitted bits in the UL, and for the DL it prints SNR, BER and total transmitted bits to each UE. This is done for each beamforming algorithm and the information can be saved to a .txt file for later comparison using the "Log to File" buttons.

5.2 UPLINK

The main task of the uplink in this model is to provide the base station with a channel estimate for each UE. To be able to reduce inter-user interference, the entire channel BW must be estimated to provide the beamforming algorithms with sufficient information. All uplink frames are built according to the scheme shown in Fig. 3. PUSCH data symbols and DM-RS symbols are placed in the grid and the DM-RS symbols are used for channel estimation as mentioned in Section 2.5. The PUSCH symbols are used as a measure of how good the channel estimator is. The model also allows transmission of multiple layers, when multiple layers are used the UEs will allocate the same time-frequency resources in the grids and each grid will be transmitted on a separate UE antenna. With the use of orthogonal pilots as explained in Section 2.5 the grids will be orthogonal to each other and this will also be true for the UE antennas. Due to this orthogonality between the antennas, the estimator at the base station will be able to estimate the link between all of the transmit and receive antenna pairs. The uplink channel estimation is then saved and later used in downlink beamforming. After estimation the grid is equalized as mentioned in Section 2.4 and the BER for the PUSCH data for each individual user is calculated to get a performance measure of the estimator.

5.3 CHANNEL

When the "Generate Channel(s)" button is pressed, the channels between all of the antenna pairs are generated as described in Section 3.1, including the Rayleigh multipath fading using Doppler spectrum and time correlation. As the "Simulate" button is subsequently pressed, the filter taps are correlated using the Kronecker

model also described in Section 3.1.3 and the signal is then filtered using a time-varying FIR filter as shown in Fig. 13 with the previously generated filter taps. At this point, the path losses and antenna gains experienced by the signal are also added. Finally, the additive white Gaussian noise (AWGN) is added on top of the received signal using the noise model described in Section 3.3. A block diagram of the program flow of the channel model in context during simulation is shown below in Fig. 15 for the uplink. The central block here is the "LTEStep" block, which performs the channel modeling and filtering. The same function "LTEStep" is also used in the same manner in the downlink but in a different context.

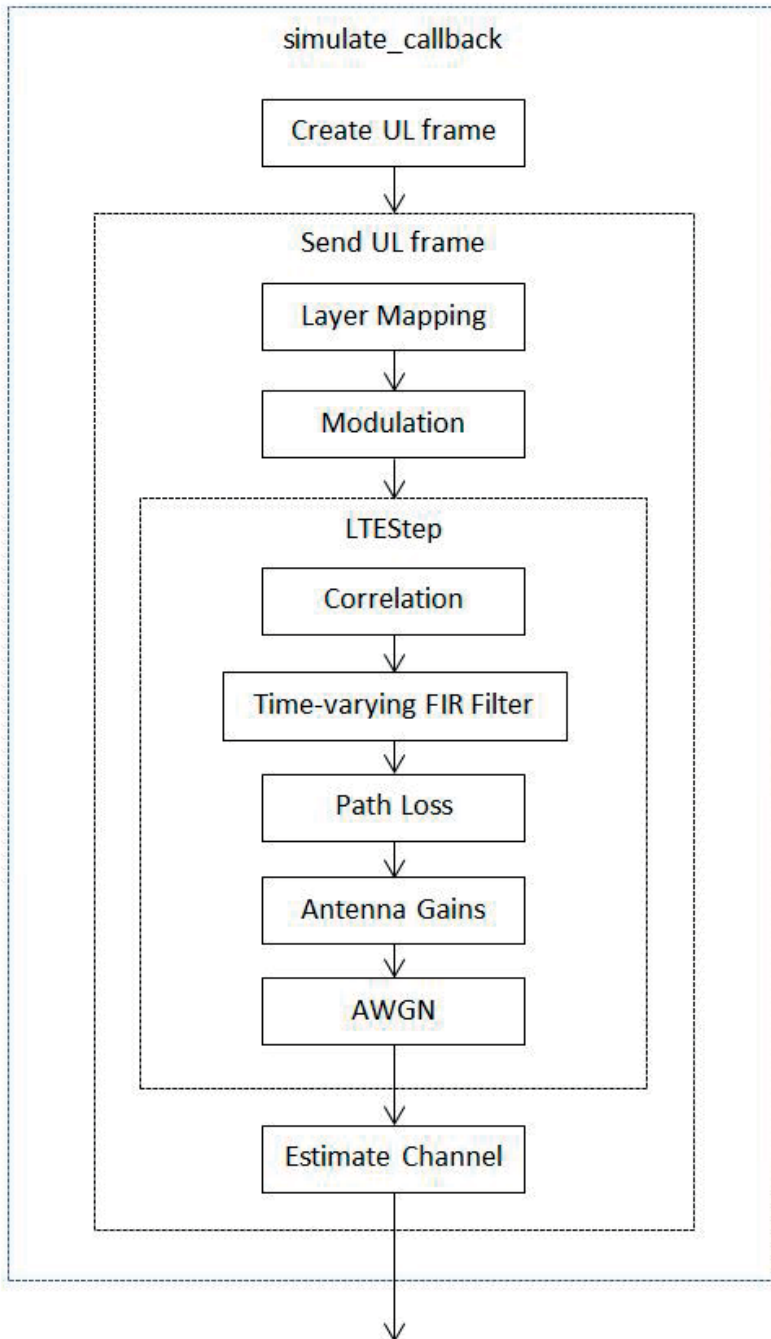


Figure 15: The program flow of the channel model, "LTEStep" in context.

5.4 DOWNLINK

The base station creates the frames and resource grids that are transmitted to the UEs in the downlink according to the scheme shown in Fig. 3. The difference compared to the uplink is that each UE is now assigned an entire grid which is filled with symbols that is intended for that specific UE. All users share the same set of reference symbols and if multiple layers are transmitted to the UEs they are separated with orthogonal reference symbols in a similar way as in the uplink. When all of the user grids are generated, they are weighted to the antennas using one of the beamforming algorithms in Section 4 before they are transmitted. Each UE uses the receiver chain as shown in Fig. 8 and the resulting constellation and BER after equalization is shown for the UEs in the GUI. The equalization is done to correct the amplitude of the received signals to make sure that the symbol demodulator works as intended as the received symbols will be of low amplitude because of the experienced path-loss. This is important for modulation of higher order than QPSK since the amplitude in the four quadrants impacts the resulting bits after demodulation.

6 RESULTS

Unless stated otherwise, all simulations are done using a channel BW of 1.4 MHz to increase the simulation speeds, especially as the same simulations are run several times to reduce the impact of the i.i.d variables in the channels. A lower BW will have the effect that the frequency diversity of the channel will decrease. This in turn means that the system could be more sensitive to frequency selectivity, however as the number of simulations increase, the effect of this will diminish because of averaging over the results. The noise also changes according to the theory in Section 3.3, however it is only relevant when the effect of noise is studied as the noise is disabled unless stated otherwise in order to study the effects of the channel alone. Other than that, a lower BW will not have any impact on the results since the reference symbols used for channel estimation and weight calculations are equally spread across the entire BW and the choice of BW is thus just a matter of the total number of symbols used. The number of UEs in the system is referred to as the number of UEs sharing the same time-frequency resource and for simplicity each UE is assigned the entire resource grid. If nothing else is mentioned the results shown in the figures of this section are the DL rates after transmission of one UL frame followed by a DL frame on the time continuous channels. Furthermore unless specified, 1 layer, 1 antenna per UE, 5 GHz carrier frequency and low correlation is used to speed up simulations.

6.1 THROUGHPUT AND VALIDATION

The throughput of the system in terms of spectral efficiency (SE) is shown for the three delay profiles EPA, EVA and ETU in Fig. 16 - Fig. 21 as the number of UEs is increased. There are two plots for each delay profile, one with QPSK and the other with 256QAM modulation. The setup for these three simulations is 32 ENB-antennas, QPSK and 256QAM modulation. Each data point is an average of ten independent runs where new channels have been generated for each run. While this number of runs is quite low, the results act as a rough estimate to show the differences of the three delay profiles and the impact of low and high modulation. To properly show this difference, the SD of the large scale fading is set to zero here. The line labeled as "Max" is the maximum theoretical throughput of the system. One can see that the algorithms deviate from the maximum as the number of UEs grows and that they perform best in EPA followed by EVA and ETU as expected from the theory in Section 3.1.2. The difference between a lower and a higher modulation order is also shown in the figures, by comparing QPSK in Fig. 16, (18 and 20 with 256QAM in Fig. 17, 19 and 21. It is seen that QPSK is more robust to the increased inter-user interference when the number of UEs is increased and does not deviate as fast from the theoretical maximum as 256QAM does. This goes in line with the theory which is explained in Section 2.2. It is also seen that there is no difference between ZF and RZF which is expected since the simulations are run in a high SNR environment and RZF will thus be the same as ZF, Section 4.3. This is the case for the results where the SNR is not specifically changed.

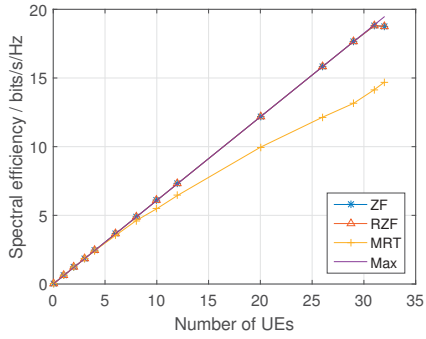


Figure 16: Spectral efficiency as a function of UEs with QPSK and 32 ENB antennas on an EPA channel.

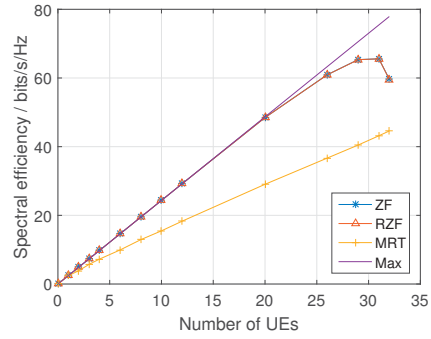


Figure 17: Spectral efficiency as a function of UEs with 256QAM and 32 ENB antennas on an EPA channel.

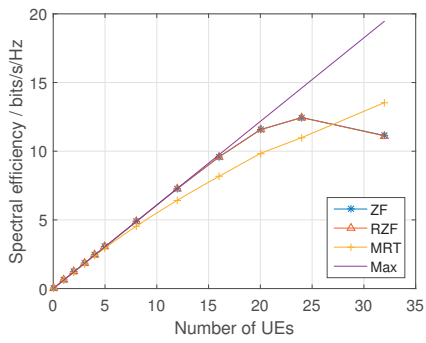


Figure 18: Spectral efficiency as a function of UEs with QPSK and 32 ENB antennas on an EVA channel.

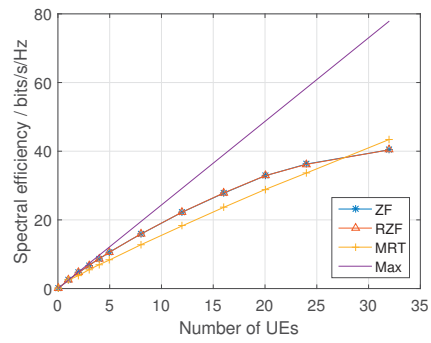


Figure 19: Spectral efficiency as a function of UEs with 256QAM and 32 ENB antennas on an EVA channel.

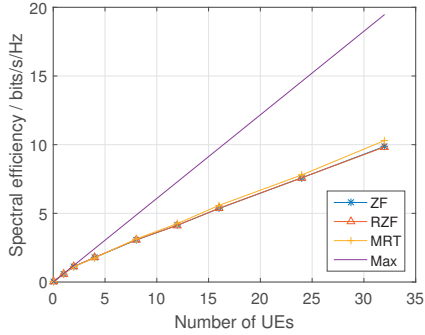


Figure 20: Spectral efficiency as a function of UEs with QPSK and 32 ENB antennas on an ETU channel.

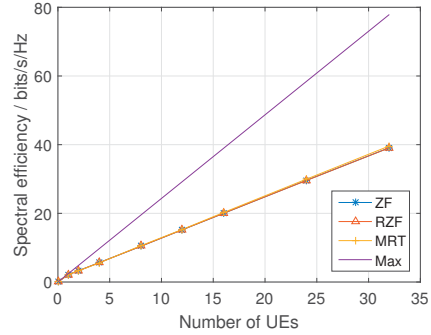


Figure 21: Spectral efficiency as a function of UEs with 256QAM and 32 ENB antennas on an ETU channel.

As the SE of the algorithms deviates from the maximum the error increases in the system. The six next figures Fig. 22 - Fig. 27 uses the same simulation setup as the six previous figures but instead of SE, the BER is plotted. The BER is a representation of the ratio between the inaccurately demodulated bits and the total number of transmitted bits. A BER of 0 % is the case where all bits are transmitted correctly and a BER around 50 % is the same as guessing, i.e. the transmission is unsuccessful. With a high BER, retransmissions are needed to provide the receiver with the necessary information and this leads to delays and slower data rates in the system. Conversely, a low enough BER can be considered as zero in a real setting because of the error correcting part in the system. As shown in Fig. 16 - Fig. 21 the SE is increased with the number of UEs but the same thing happens for the BER in Fig. 22 - Fig. 27. Therefore the number of UEs sharing the same resources has to be chosen carefully to get a good trade-off between SE and BER to avoid retransmissions and achieve maximum rates in the system. As also shown in Fig. 22 - Fig. 27, the BER differs between the delay profiles and an adaptive measure is needed to account for this. Note that the data points that are not present in the BER plots indicates that there are no errors for those points as the BER is plotted in a logarithmic scale.

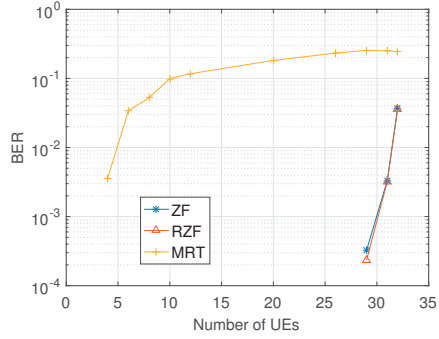


Figure 22: BER as a function of UEs with QPSK and 32 ENB antennas on an EPA channel.

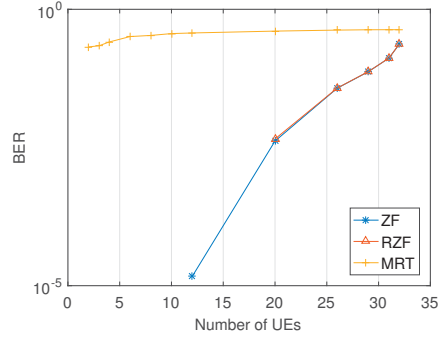


Figure 23: BER as a function of UEs with 256QAM and 32 ENB antennas on an EPA channel.

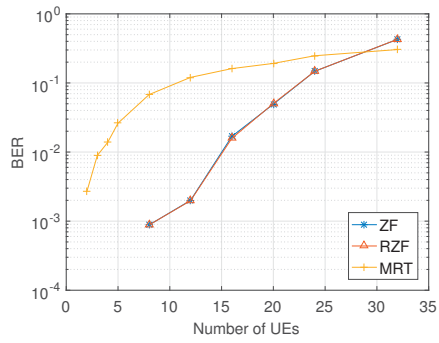


Figure 24: BER as a function of UEs with QPSK and 32 ENB antennas on an EVA channel.

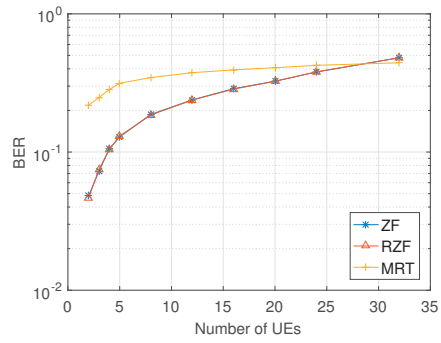


Figure 25: BER as a function of UEs with 256QAM and 32 ENB antennas on an EVA channel.

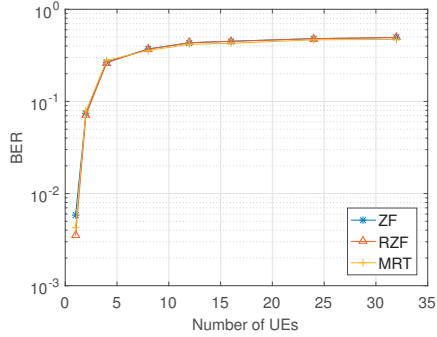


Figure 26: BER as a function of UEs with QPSK and 32 ENB antennas on an ETU channel.

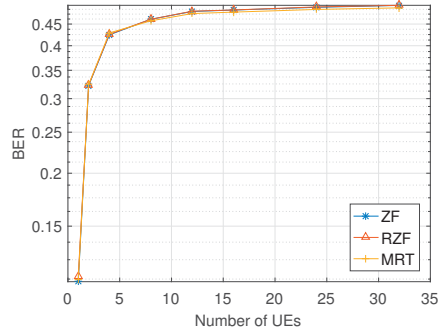


Figure 27: BER as a function of UEs with 256QAM and 32 ENB antennas on an ETU channel.

6.2 PERFORMANCE IN MASSIVE MIMO

In the results of Fig. 28 - Fig. 30 it is shown how the SE changes with the number of ENB-antennas for a constant number of UEs with the three delay profiles. The setup for these simulations is 4 UEs and QPSK modulation. It is seen that EPA and EVA reaches the maximum throughput at around 8 ENB-antennas for ZF and at 32 ENB-antennas for MRT. In ETU all three algorithms have similar performance in this setup and is almost at maximum throughput at 350 ENB-antennas. This matches with the result from (24), which says that the system performance increases with the number of base station antennas. To properly see the difference between the delay profiles, large scale fading SD is again set to zero.

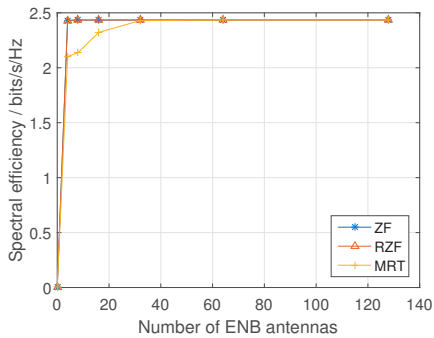


Figure 28: Spectral efficiency for 4 UEs with QPSK on an EPA channel as the number of ENB antennas grows.

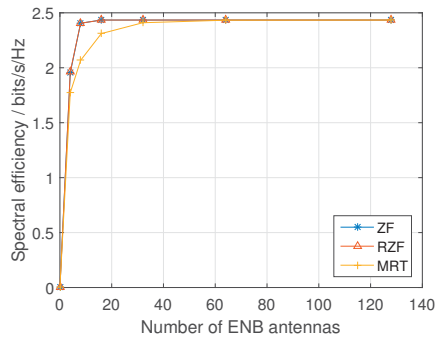


Figure 29: Spectral efficiency for 4 UEs with QPSK on an EVA channel as the number of ENB antennas grows.

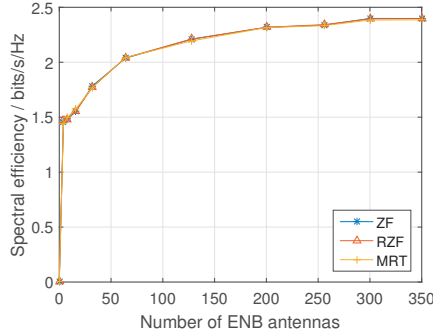


Figure 30: Spectral efficiency for 4 UEs with QPSK on an ETU channel as the number of ENB antennas grows.

6.3 MULTI-LAYER TRANSMISSION

The SE of the system will also depend on the number of layers that are being transmitted at the same time, as more layers increase the number of resource grids that are transmitted. We should therefore expect almost a 1:1 ratio between the number of layers and the SE. As the channel is slower and more antennas are being used, the noise is kept at a minimum. This produces an almost linear increase in SE when the number of layers is increased as shown in Fig. 31 using 32 base station antennas and an EPA profile. Moreover, for Fig. 31 - Fig. 34 4 users are used at a small distance of [100 m, 100 m] in a two-dimensional grid with 1 antenna per user and QPSK modulation. The results are averaged over 50 independent runs. To properly evaluate the effect of different channels and different number of antennas, the large scale fading variance is set to zero.

As the channel affects the signal more adversely, more layers become comparably more inefficient as it is more difficult to separate them with the decreased accuracy of the beamforming as explained in Section 2.3. Fig. 32 also supports this. The same behaviour is shown with 16 antennas in Fig. 33 and Fig. 34, but as the limit on the number of UEs and layers is met as shown in Fig. 34, the SE drastically worsens when the delay profiles are compared. Additionally, ZF in this case is outperformed by both RZF and MRT because of the sensitivity of ZF to erroneous channel estimates [30]. Worth noting is that the BER for the worst case shown in Fig. 34 using 4 layers and 4 users is around 40 % even for the RZF and therefore not practical for real transmissions. The BER could however be improved by increasing the number of base station antennas as shown in Fig. 28 - Fig. 30.

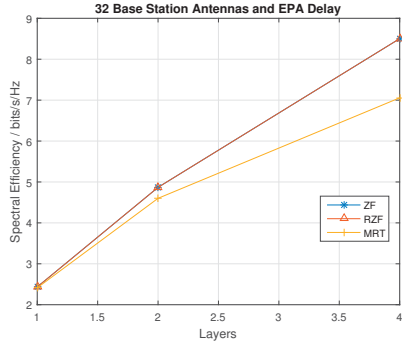


Figure 31: Spectral efficiency for 4 UEs using QPSK and 32 antennas on an EPA channel as the number of layers increases.

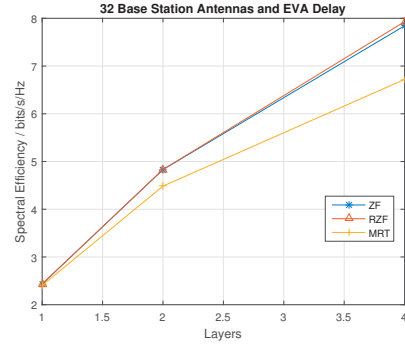


Figure 32: Spectral efficiency for 4 UEs using QPSK and 32 antennas on an EVA channel as the number of layers increases.

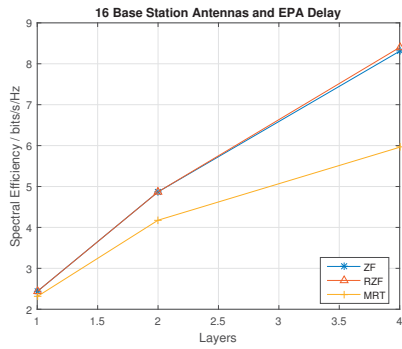


Figure 33: Spectral efficiency for 4 UEs using QPSK and 16 antennas on an EPA channel as the number of layers increases.

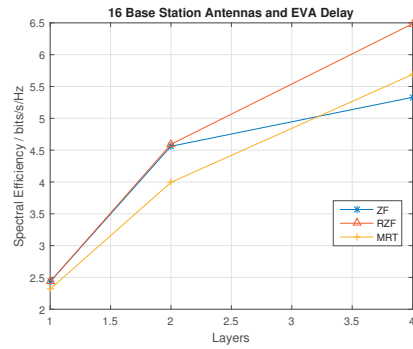


Figure 34: Spectral efficiency for 4 UEs using QPSK and 16 antennas on an EVA channel as the number of layers increases.

6.4 TRANSMISSION OF CONSECUTIVE FRAMES

To see for how long the beamforming weights are valid in the different delay profiles, a time-correlated channel spanning ten subframes is generated and one UL frame followed by nine DL frames are transmitted on the channel. The following parameters are used in this setup; 32 ENB-antennas, 4 single antenna UEs, QPSK modulation and zero large scale fading SD to properly compare the delay profiles. Fig. 35 - Fig. 36 shows how the BER changes with the number of consecutive DL frames in the delay profiles EVA and ETU. For the EPA channel the beamforming weights give no errors for at least 9 subframes for all algorithms with this setup and is thus not plotted. As expected it is worse for the EVA profile as shown in Fig. 35 where the error is only zero or close to zero for two subframes for the algorithms. With this setup the performance

is unsatisfactory for all the subframes in the ETU profile as shown in Fig. 36, though the two first frames are better than the ones following. Due to the random nature of the channel and the fading as explained in Section 3.1.1, the BER can also periodically improve as more DL frames are sent using the same estimates as shown in Fig. 36. Again, a missing data point means a BER of zero.

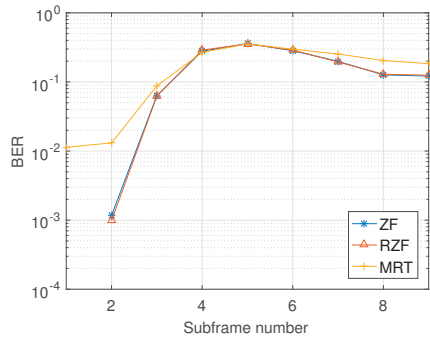


Figure 35: The DL BER with QPSK on an EVA channel as a function of consecutive DL frames.

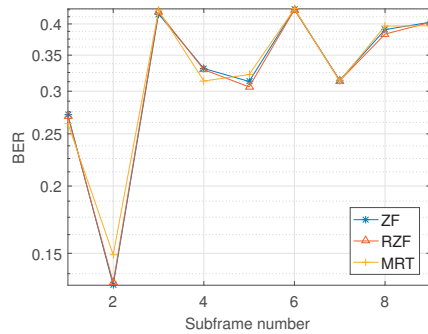


Figure 36: The DL BER with QPSK on an ETU channel as a function of consecutive DL frames.

As the two first subframes had the lowest BER in the EVA and ETU profiles, another simulation is done on a 15-subframe long channel where the weights are now updated every third subframe, i.e. looping the frame pattern of UL-DL-DL five times. The resulting DL BER is shown in Fig. 37 and Fig. 38 for EVA and ETU respectively. As is expected, the BER is significantly lower when the beamforming weights are updated regularly to adapt to the changes of the time-varying channel.

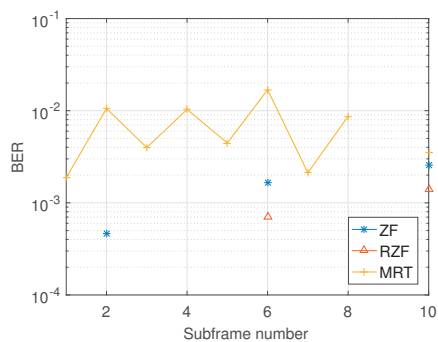


Figure 37: The DL BER using QPSK on an EVA channel as a function of subframes when the weights are updated every third subframe.

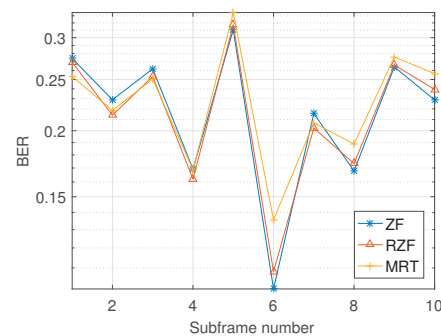


Figure 38: The DL BER using QPSK on an ETU channel as a function of subframes when the weights are updated every third subframe.

6.5 ALGORITHM COMPLEXITY

The computation times for the ZF and MRT algorithms as a function of the number of UEs and ENB antennas are shown in Fig. 39. They are measured as an average of 50 runs in Matlab during run time on a PC running Windows and are thus not exact. However the results show that the ZF-algorithms and MRT algorithms grow linearly in complexity and that MRT is significantly faster than ZF. The average ratio between the two algorithms gives that MRT is about 16.8 times faster than ZF, with the gap increasing for larger systems.

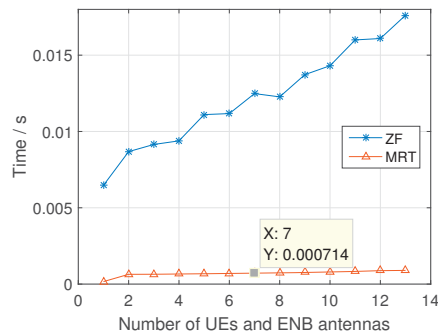


Figure 39: Computation time as the number of UEs and ENB antennas grows.

6.6 EFFECTS OF CHANNEL DISCREPANCIES BETWEEN USERS

A phenomenon that arises when all users are sharing the same frequencies is that users with different channel conditions, for example different path loss, will experience a higher BER than users with similar conditions. Most notably, this mostly occurs for the ZF algorithms as shown in the constellations diagrams in Fig. 40 - Fig. 45. Illustrated below is also to what extent simply changing the distance of one of the users affects the received constellations. The settings for these tests are a 20 MHz bandwidth, 32 base station antennas, EVA delay profile, 16QAM modulation and varying distance. To show this effect, large scale fading SD is set to zero since it would otherwise affect the users independently and possibly nullify or amplify the results from these tests.

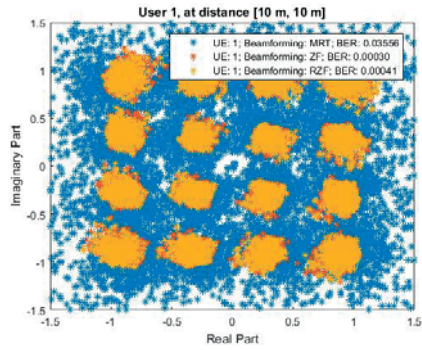


Figure 40: Received constellation of user 1 in a system with two users close to the base station.

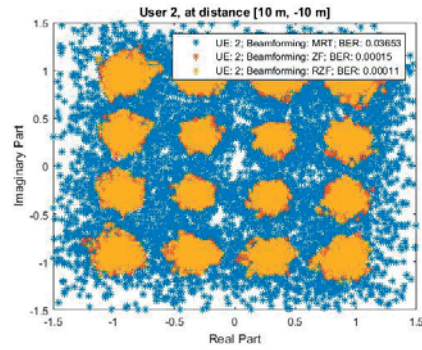


Figure 41: Received constellation of user 2 in a system with two users close to the base station.

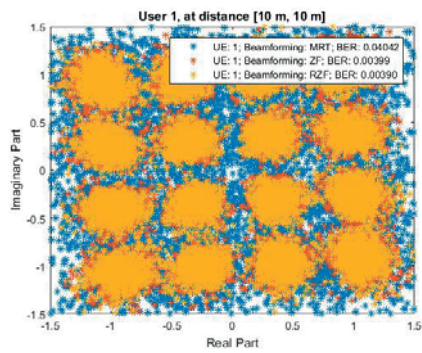


Figure 42: Received constellation of user 1 in a system with one user close to the base station and one further away.

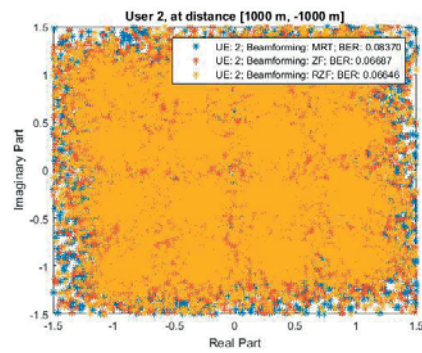


Figure 43: Received constellation of user 2 in a system with one user close to the base station and one further away.

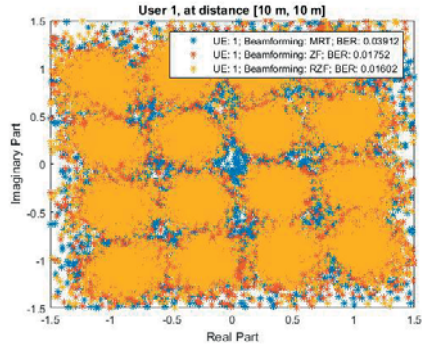


Figure 44: Received constellation of user 1 in a system with one user close to the base station and one very far away.

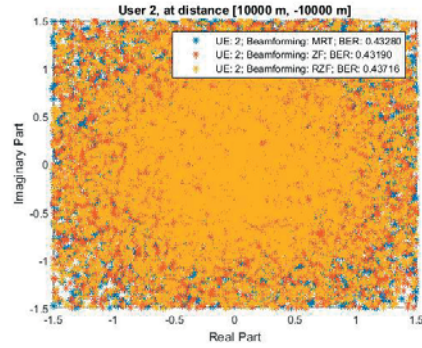


Figure 45: Received constellation of user 2 in a system with one user close to the base station and one very far away.

6.7 ALGORITHM PERFORMANCE AND SNR

In these simulations the three algorithms' performance for different SNR is investigated and the result is an average of 50 runs. The performance for a system with 4 and 32 base station antennas is shown in Fig. 46 and Fig. 47 respectively. The other parameters for this simulation are; 4 UEs, QPSK Modulation, EPA profile, low correlation and zero antenna-, UE-, and eNB-gain. The gains are set to zero to get a better average of the SNR estimate and the average SNR is changed by changing the distance to the UEs. The large scale fading SD is also set to zero to further isolate the performance to SNR connection. It is shown in Fig. 46 that RZF and MRT have similar performance in the low SNR range while RZF and ZF have similar performance in the high SNR range. In between low and high SNR, RZF outperforms the other algorithms and this is supported by the theory in Section 4.3. In other words, for a system with low SNR it is important to maximize the SNR and for a system with high SNR it is more important to maximize the SINR. In Fig. 47 the inter-user interference of the system is lower because of the increased number of base station antennas from the theory in Section 4.4. The results that follows from this is that RZF follows ZF in the entire SNR range as shown in Fig. 47, because maximum throughput is gained from maximizing the SINR. The throughput of MRT is also increased because of the increased orthogonality of the system.

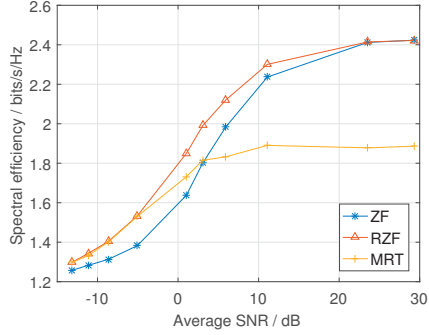


Figure 46: 4 base station antennas.

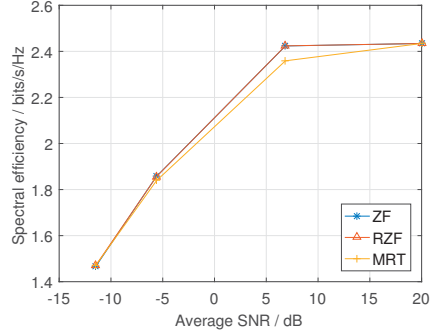


Figure 47: 32 base station antennas.

6.8 ANTENNA CORRELATION

To demonstrate how the correlation parameter affects the throughput, simulations are done with low, medium and high correlation which is specified in Section (3.1.3). The simulations are run with the following setup; 16 ENB Antennas, 2 layers, 2 UE antennas, 2 UEs, EPA profile and 16QAM modulation. To see the effect of the correlation more separately, large scale fading SD is zero here. The throughput as the total number of correctly received bits is seen in Table 5, and the result is an average of 50 runs. As expected the throughput is lower with more correlation because the inter-user interference is increased. It is also seen that the ZF algorithms handles the increased interference better than MRT.

	Low	Medium	High	Max Throughput
ZF	6816	6810.78	6747.52	6816
RZF	6816	6811.14	6746.02	6816
MRT	5867.44	4100.7	3957.64	6816

Table 5: Throughput for the three specified correlations.

6.9 MOBILITY

Given the layout of the pilot symbols and the length of one subframe as mentioned in Section 2.5 and the coherence time of the channel as in Section 3.4, the maximum mobility the beamforming can handle can be calculated. The maximum updating frequency of the weights is when every second frame is an UL subframe, which means every 14th symbol. Since the pilots are placed in symbol 4 and 11 of the UL subframe, there are also 3 symbols at the end of the UL subframe during which the channel can change. Therefore the weights need to be valid for at least 17 symbols of approximately $71 \mu\text{s}$ each, which is approximately 1.2 ms in total. Using (11) in Section 3.4 and the Nyquist sampling theorem, the minimum sampling period is

given as

$$T_{min} = \sqrt{\frac{9}{16\pi * 2f_d^2}} \quad (26)$$

where f_d is the maximum Doppler frequency [31]. If the total time for the 17 symbols (1.2 ms) is inserted into (26), the approximate maximum Doppler frequency allowed for a coherent channel is 174.85 Hz.

The simulations are run with 10 ENB antennas, 2 UEs and QPSK modulation over an average of 200 runs. Furthermore, zero large scale fading SD is used to properly relate the performance to the theory in Section 3.4. The SE is shown in Fig. 48 as the Doppler frequency is increased, and the throughput is at max for low frequencies and starts to decrease after 100 Hz. Although the decrease is slow at first and only picks up at around 150 Hz.

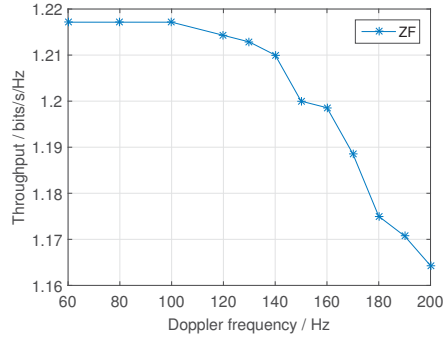


Figure 48: SE plotted against Doppler frequency.

6.10 EFFECTS OF LARGE SCALE FADING

Thus far, the large scale fading has been inactivated to properly see the effects of different parameters. However as this effect can have a standard deviation of as much as 4-10 dB independently per user as in Section 3.1.4, the performance could see a noticeable change when it is present. The spread of the large scale fading is shown in Fig. 49 and Fig. 50 for a standard deviation of 4 dB and 10 dB respectively. The mean of the large scale fading is the path loss, which is set to -100 dB for this setup.

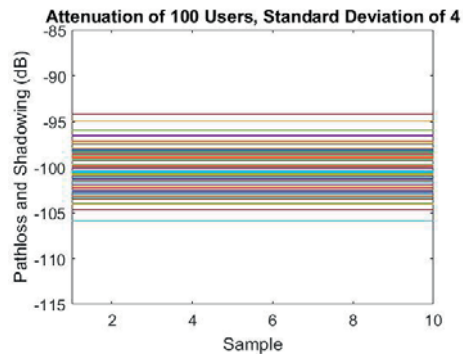


Figure 49: Spread of the large scale fading around a mean path loss of -100 dB and a standard deviation of 4 dB.

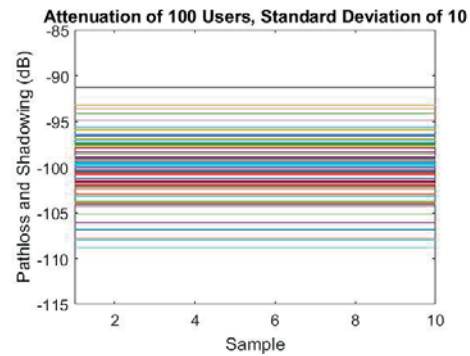


Figure 50: Spread of the large scale fading around a mean path loss of -100 dB and a standard deviation of 10 dB.

As can be seen, the effective attenuation of each user can be increased or decreased by the large scale fading. Most importantly, the effect is independent for each user meaning that users at the same distance do not necessarily experience the same SNR. This in combination with what is shown in Section 6.6 could give rise to slightly worse beamforming performance if the difference between users is significant enough.

7 DISCUSSION

As mentioned in Section 3.1.3, the model used for correlating the channels might not be inherently valid for large arrays [19]. Despite this, the Kronecker model is widely used in the LTE standard [4] for this very purpose. The effect of this should present itself once massive MIMO [2] becomes more prevalent and detailed models are needed. Especially in beamforming situations where the antennas can be expected to be placed fairly closely together which means that the correlation is higher. However the Kronecker model is simple to implement and a good starting point for the model in this work, considering the goals set in Section 1.1.

Regarding the results in Section 6, one can see that almost every parameter is a compromise between robustness and throughput. Both more layers and more UEs require better channel estimates to reach full potential since the respective channels need to be separated to be properly decoded. As the channel changes, this initial estimate becomes a worse fit which means that the beamforming performance also deteriorates with time. To combat the deteriorating channel estimate, a new estimate could be performed but at the cost of DL data rate since the system requires UL transmissions to do so.

As shown in Section 6.6, having users with different channels may cause some users to experience a worse BER than if they are modeled independently. This is an effect of the fact that all users currently use the entire resource grid. One way to get around this would be to split the resource grid between users so that some users exclusively use certain frequencies. Groups could also be made so that users with similar channel conditions share the same frequencies. This also opens up possibilities of different estimate updating frequencies for different groups, which in turn increases the possible DL data rate for users with slower fading channels. It then follows that it could be of interest to expand the current model to include the possibility of users with different channel conditions and as well as SNR.

Since the channel estimates need to be readily available to the transmitter for beamforming, they need to be stored on the DSP. The storage needs will then depend on how many weights are needed to achieve good beamforming. For channels which are relatively flat in frequency, one weight per subcarrier may leave some weights redundant which could potentially at least halve the needed weights. This is completely dependent on the channel and could be a parameter varying with the frequency selectivity of the channel. It could potentially also be a parameter independent for each group of users, similar to how some users may need more frequent channel estimates when the grid is split between the users as above.

When looking at the performance of the algorithms from the results in Section 6 one can see that the ZF based algorithms performs better than MRT when there are many users in the system transmitting on relatively flat channels. On the other hand the complexity of MRT is much lower than the one of ZF and this is very crucial in LTE where transmissions are done every symbol, which is about $71 \mu s$. Since the current simulations are done in Matlab, little can be said about whether either of the algorithms are capable of computing within a single symbol. Another advantage of MRT in terms of complexity is that the computations can be parallelized and done on each antenna element individually, since the user weighting to each antenna

is just using the specific antenna channel estimate. Furthermore the performance also depends on the number of base station antennas and users sharing the same resources, which is a design related topic. A complexity reduced ZF (CRZF) algorithm is proposed in [32] which starts from the MRT solution and cancels out the N worst inter-user interferers. As a theoretical result of this the complexity of the CRZF was shown to be 2-7% of the original ZF while still keeping 90% of its performance. This sounds very promising and should be further investigated.

Lastly, an idea for improving the current testing environment would be to include a surface plot in the layout plot, showing the signal strength at every point in space. This way one might see whether the algorithms provide correct beamforming through analysis of the signal strength at different points. It could also serve as an educational tool, showing the differences of MRT and ZF in terms of interference cancelling.

7.1 CONCLUSION

In this work we have successfully built a model with the functionality stated in Section 5.1. The model also meets the requirements for investigating the statements in Section 1.1 (Purpose & Aims) of this thesis. We have been able to find a way of weighting the DL grids to the antennas and transmit the grids over a wireless channel. The algorithms MRT, ZF and RZF have been compared in different settings and it is seen that MRT is less complex than the ZF algorithms. The ZF algorithms on the other hand are more robust to increased inter-user interference as many users transmit in the same system. It is also seen that RZF outperforms MRT and ZF in the entire SNR range and we have been able to beamform up to four layers to each UE in the system. As a summary, the objectives have been met and the initial questions have been investigated and answered.

7.2 FUTURE WORK

If we were to continue work on this project, a first step would be to implement the complexity reduced zero-forcing algorithm and further study the complexity of all the algorithms by implementing them in a real setting, where the computing times can be accurately compared. Further improvements would be to find an adaptive algorithm that calculates the number of UEs that should share the same resources as this is dependent on the channel conditions. Implementing adaptive weight updating both in time and frequency would also be of interest. Finally improvements to the channel model would be investigated, specifically the spatial correlation for large antenna arrays and the inclusion of a Rician fading model to cover more simulation cases.

REFERENCES

- [1] Mathworks, "*LTE System Toolbox Release 2016a*", Natick, Massachusetts, United States, 3 March 2016.
- [2] E. G. Larsson, O. Edfors, F. Tufvesson, T. L. Marzetta and B. Labs "*Massive MIMO for Next Generation Wireless Systems*", IEEE Communications Magazine, Volume 52, Issue 2, February 2014.
- [3] J. Vieira, S. Malkowsky, K. Nieman, Z. Miers, N. Kundargi, L. Liu, I. Wong, V. Öwall, O. Edfors and F. Tufvesson, "*A flexible 100-antenna testbed for Massive MIMO*", 2014 IEEE Globecom Workshop - Massive MIMO: From Theory to Practice, Austin, Texas, USA, 2014-12-08.
- [4] 3GPP, <http://www.3gpp.org/>.
- [5] C. Johnson, "*Long Term Evolution IN BULLETS 2nd Edition*", LTE-BULLETS 2012.
- [6] E. Dahlman, S. Parkvall and J. Sköld, "*4G LTE/LTE-Advanced for Mobile Broadband 2nd Edition*", Elsevier Ltd. 2014.
- [7] H. Zarrinkoub, "*Understanding LTE with MATLAB: From Mathematical Modeling to Simulation and Prototyping*", John Wiley & Sons, Ltd 2014.
- [8] Photograph, viewed 28 April 2016, <http://se.mathworks.com/help/lte/ug/fdd-and-tdd-duplexing.html>.
- [9] 3GPP, TS 36.211 version 13.1.0 Release 13, March 2016.
- [10] Y. Jiang, M. K. , Varansi and J. Li, "*Performance Analysis of ZF and MMSE Equalizers for MIMO Systems: An In-Depth Study of the High SNR Regime*", IEEE Transactions on Information Theory, Vol. 57, April 2011
- [11] H.J. Zepernick and A. Finger, "*Pseudo Random Signal Processing: Theory and Application*", John Wiley & Sons, 2013
- [12] A. Holst and V. Ufnarovski, "*Matrix Theory*", Studentlitteratur 2014 pp. 302.
- [13] Photograph, viewed 6 June 2016, <http://se.mathworks.com/help/lte/examples/dl-sch-and-pdsch-processing-chain.html>.
- [14] Mathworks, "*Channel Estimation*" viewed 6 June 2016, <http://se.mathworks.com/help/lte/ug/channel-estimation.html>
- [15] X. Hou and H. Kayama, "*Demodulation Reference Signal Design and Channel Estimation for LTE-Advanced Uplink*", published in M. Almeida "*Advances in Vehicular Networking Technologies*", 11 April 2011.
- [16] Y. R. Zheng and C. Xiao, "*Simulation Models With Correct Statistical Properties for Rayleigh Fading Channels*", IEEE Transactions on Communications, Vol. 51, No. 6, June 2003.

- [17] D. J. Young and N. C. Beaulieu, "*The Generation of Correlated Rayleigh Random Variates by Inverse Discrete Fourier Transform*", IEEE Transactions on Communications, Vol. 48, No. 7, July 2000.
- [18] 3GPP, TS 36.101 version 9.12.0 Release 9, July 2012.
- [19] C. Oestges, "*Validity of the Kronecker Model for MIMO Correlated Channels*", IEEE 63rd Vehicular Technology Conference, Vol. 6, May 2006.
- [20] DS. Shiu, G. J. Foschini, M. J. Gans and J. M. Kahn "*Fading Correlation and Its Effect on the Capacity of Multielement Antenna Systems*", IEEE Transactions on Communications, Vol. 48, No. 3, March 2000.
- [21] A. F. Molisch, "*Wireless Communications*", John Wiley & Sons, 2005
- [22] WINNER project, "*IST-4-027756 WINNER II D 1.1.2 v1.2, WINNER II Channel Models*", <https://www.ist-winner.org>, 2006.
- [23] H. Nyquist, "*Thermal Agitation of Electric Charge in Conductors*", Physical Review Vol. 32, July 1928.
- [24] T. S. Rappaport, "*Wireless Communications: Principles and Practice*", 2nd Edition, Prentice Hall, 2002
- [25] Tipler P. A. and Mosca G. P., Physics for scientists and engineers. New York, W.H. Freeman 2003.
- [26] X. Gao, Doctoral Thesis: "*Massive MIMO in Real Propagation Environments*", Lund University, January 2016.
- [27] D. HN. Nguyen and T. Le-Ngoc, "*MMSE precoding for multiuser MISO downlink transmission with non-homogeneous user SNR conditions*" EURASIP Journal on Advances in Signal Processing, 6 June 2014.
- [28] M. Sadek, A. Tarighat and A. H. Sayed, "*A Leakage-Based Precoding Scheme for Downlink Multi-User MIMO Channels*", IEEE Transactions on Wireless Communications, Volume 6, 21 May 2007.
- [29] M. Ghosh, "*A Comparison of Normalizations for ZF Precoded MU-MIMO Systems in Multipath Fading Channels*", IEEE Wireless Communications Letters, Volume 2, 2013.
- [30] C. Wang, E. K. S. Au, R. D. Murch and V. K. N. Lau, "*Closed-Form Outage Probability and BER of MIMO Zero-Forcing Receiver in the Presence of Imperfect CSI*", IEEE 7th Workshop on Signal Processing Advances in Wireless Communication, July 2006
- [31] R. P. Jover, "*LTE PHY Fundamentals*", viewed 11 June 2016, http://www.ee.columbia.edu/~roger/LTE_PHY_fundamentals.pdf
- [32] CS. Park, YS. Byun, A. M. Bokiye and YH. Lee, "*Complexity Reduced Zero-Forcing Beamforming in Massive MIMO Systems*", Information Theory and Applications Workshop (ITA), 9-14 February 2014.



LUND
UNIVERSITY

Series of Master's theses
Department of Electrical and Information Technology
LU/LTH-EIT 2016-546
<http://www.eit.lth.se>